NAVAL POSTGRADUATE SCHOOL

MONTEREY, CALIFORNIA

THESIS

EVALUATION OF DAYTIME BOUNDARY LAYER HEIGHTS FROM A MESOSCALE MODEL USING PROFILERS/RASS MEASUREMENTS

by

Lindsay A. Bloch

March 2008

Thesis Advisor: Qing Wang
Second Reader: Wendell A. Nuss

Approved for public release; distribution is unlimited.

THIS PAGE INTENTIONALLY LEFT BLANK

REPORT DOCUMENTATION PAGE			*Form Approved OMB No. 0704-0188*
Public reporting burden for this collection of information is estimated to average 1 hour per response, including the time for reviewing instruction, searching existing data sources, gathering and maintaining the data needed, and completing and reviewing the collection of information. Send comments regarding this burden estimate or any other aspect of this collection of information, including suggestions for reducing this burden, to Washington headquarters Services, Directorate for Information Operations and Reports, 1215 Jefferson Davis Highway, Suite 1204, Arlington, VA 22202-4302, and to the Office of Management and Budget, Paperwork Reduction Project (0704-0188) Washington DC 20503.

1. AGENCY USE ONLY *(Leave blank)*

2. REPORT DATE
March 2008

3. REPORT TYPE AND DATES COVERED
Master's Thesis

4. TITLE AND SUBTITLE Evaluation of Daytime Boundary Layer Heights from a Mesoscale Model Using Profilers/RASS Measurements

5. FUNDING NUMBERS

6. AUTHOR(S) Lindsay A. Bloch

7. PERFORMING ORGANIZATION NAME(S) AND ADDRESS(ES)
Naval Postgraduate School
Monterey, CA 93943-5000

8. PERFORMING ORGANIZATION REPORT NUMBER

9. SPONSORING /MONITORING AGENCY NAME(S) AND ADDRESS(ES)
N/A

10. SPONSORING/MONITORING AGENCY REPORT NUMBER

11. SUPPLEMENTARY NOTES The views expressed in this thesis are those of the author and do not reflect the official policy or position of the Department of Defense or the U.S. Government.

12a. DISTRIBUTION / AVAILABILITY STATEMENT
Approved for public release; distribution is unlimited.

12b. DISTRIBUTION CODE

13. ABSTRACT (maximum 200 words)

This thesis study focuses on the evaluation of the boundary layer height (BLH) diagnosed from a mesoscale model in comparison to wind profiler/Radio Acoustic Sounding System (RASS) measurements from the profiler site at Miramar Marine Corps Station (MMR). This objective is met through validation of the observed BLH and evaluations of the model BLH using the observed BLH's. In particular, two methods, one uses Signal-to-Noise-Ratio (SNR) from the profiler, and the other uses the vertical gradient of virtual potential temperature from RASS, were developed to detect BLH from the profiler/RASS systems. The detected BLH was validated against BLH from rawinsonde measurements. The SNR method gives a better mean BLH in the clear convective unstable BL's while the gradient method shows better correlation with the rawinsonde BLH. The Weather Research and Forecasting (WRF) model for the inland location (MMR) was compared to these profiler BLH estimates. Although WRF reasonably predicts the general BL behavior, WRF underestimated the BLH by several hundred meters. The WRF diagnosed BLH using the bulk Richardson number was inconsistent with the WRF predicted BL thermodynamics structure. An alternative BLH detection scheme using a gradient method of BLH detection is proposed and tested for WRF, showing better results.

14. SUBJECT TERMS Marine Atmosphere Measurement Lab (MAML), Wind profiler/Radio Acoustic Sounding System (RASS), boundary layer height (BLH), Weather Research and Forecasting model (WRF)

15. NUMBER OF PAGES
91

16. PRICE CODE

17. SECURITY CLASSIFICATION OF REPORT Unclassified	**18. SECURITY CLASSIFICATION OF THIS PAGE** Unclassified	**19. SECURITY CLASSIFICATION OF ABSTRACT** Unclassified	**20. LIMITATION OF ABSTRACT** UU

NSN 7540-01-280-5500

Standard Form 298 (Rev. 2-89)
Prescribed by ANSI Std. 239-18

THIS PAGE INTENTIONALLY LEFT BLANK

Approved for public release; distribution is unlimited

EVALUATION OF DAYTIME BOUNDARY LAYER HEIGHTS FROM A MESOSCALE MODEL USING PROFILERS/RASS MEASUREMENTS

Lindsay A. Bloch
Captain, United States Air Force
B.S., The Pennsylvania State University, 2002

Submitted in partial fulfillment of the
requirements for the degree of

MASTER OF SCIENCE IN METEOROLOGY

from the

NAVAL POSTGRADUATE SCHOOL
March 2008

Author: Lindsay A. Bloch

Approved by: Qing Wang
                  Thesis Advisor

                  Wendell A. Nuss
                  Second Reader

                  Philip A. Durkee
                  Chairman, Department of Meteorology

THIS PAGE INTENTIONALLY LEFT BLANK

ABSTRACT

This thesis study focuses on the evaluation of the boundary layer height (BLH) diagnosed from a mesoscale model in comparison to wind profiler/Radio Acoustic Sounding System (RASS) measurements from the profiler site at Miramar Marine Corps Station (MMR). This objective is met through validation of the observed BLH and evaluations of the model BLH using the observed BLH's. In particular, two methods, one uses Signal-to-Noise-Ratio (SNR) from the profiler, and the other uses the vertical gradient of virtual potential temperature from RASS, were developed to detect BLH from the profiler/RASS systems. The detected BLH was validated against BLH from rawinsonde measurements. The SNR method gives a better mean BLH in the clear convective unstable BL's while the gradient method shows better correlation with the rawinsonde BLH. The Weather Research and Forecasting (WRF) model for the inland location (MMR) was compared to these profiler BLH estimates. Although WRF reasonably predicts the general BL behavior, WRF underestimated the BLH by several hundred meters. The WRF diagnosed BLH using the bulk Richardson number was inconsistent with the WRF predicted BL thermodynamics structure. An alternative BLH detection scheme using a gradient method of BLH detection is proposed and tested for WRF, showing better results.

THIS PAGE INTENTIONALLY LEFT BLANK

TABLE OF CONTENTS

LIST OF FIGURES

THIS PAGE INTENTIONALLY LEFT BLANK

LIST OF TABLES

THIS PAGE INTENTIONALLY LEFT BLANK

LIST OF ACRONYMS AND ABBREVIATIONS

3DVAR	Three-Dimensional Variational data assimilation system
ABL	Atmospheric Boundary Layer
AFWA	Air Force Weather Agency
ARW	Advanced Research Weather
ASL	Above Sea Level
ATD	Atmospheric Transport and Dispersion
BL	Boundary Layer
BLH	Boundary Layer Height
BLP	Boundary Layer Profile
CBRNE	Chemical, Biological, Radiological, Nuclear, and High Yield Explosive
CBL	Convective Boundary Layer
CDF	Cumulative Distribution Function
cm	centimeter
CO_2	carbon dioxide
COAMPS	Navy's Coupled Atmospheric Prediction System
CONUS	Continental United States
D2PUFF	DoD certified Lagrangian Gaussian D2-Puff model
DoD	Department of Defense
DOY	Day of Year
EZ	Entrainment Zone
FA	Free Atmosphere
FAA	Federal Aviation Administration
FAST	Fourier Amplitude Sensitivity Test
FSL	Forecast Systems Laboratory
hPa	hectapascal
HPAC	Hazard and Prediction Assessment Capability
Kh	Kelvin-Helmholtz instability
kHz	kilohertz
km	kilometer
KMA	Korean Meteorological Administration
LAX	Los Angeles IAP profiler site
LSM	Land Surface Model
LW	long wave
m	meter
m/s	meters per second
MAML	Marine Atmospheric Measurement Lab
MHz	megahertz
ML	Mixed Layer
MM5	The Fifth-Generation NCAR / Penn State Mesoscale Model
MMR	Miramar profiler site
MOV	profiler site
MR	Mixing Ratio

MRF	Medium Range Forecast
MYJ	Mellor-Yamada-Janjic
NAM	North American Model
NCAR	National Center for Atmospheric Research
NCEP	National Centers for Environmental Predictions
NOAA	National Oceanic and Atmospheric Administration
NPS	Naval Postgraduate School
O_3	ozone
ONT	Ontario Airport profiler site
ORD	Fort Ord
PBL	Planetary Boundary Layer
PDF	Probability Distribution Function
PSU	The Pennsylvania State University
q	specific humidity
RAOB	Radiosonde Observations
RASS	Radio Acoustic Sounding System
RDAPS	Regional Data Assimilation and Prediction System
Ri	Richardson number
Ri_b	bulk Richardson number
RL	Residual Layer
RRTM	Rapid Radiative Transfer Model
SBL	Stable Boundary Layer
SCIPUFF	Second-order Closure Integrated Gaussian Puff model
SIM	Simi Valley profiler site
SL	Surface Layer
SNR	Signal-to-Noise Ratio
SW	shortwave
T	temperature
T_v	virtual temperature
TKE	Turbulent Kinetic Energy
U or u	component of wind in the x direction
UTC	Universal Time Coordinate
W or w	component of wind in the y direction
WRF	Weather Research and Forecasting model
YSU	Yonsei University
Z or h	height coordinate
Zi or zi	height of the mixed layer
θ	potential temperature
θ_v	virtual potential temperature

ACKNOWLEDGMENTS

THIS PAGE INTENTIONALLY LEFT BLANK

I. INTRODUCTION

A. BASICS OF THE ATMOSPHERIC BOUNDARY LAYER (ABL)

The atmospheric boundary layer (ABL) is defined as the part of the troposphere that is directly influenced by the presence of the earth's surface, and responds to surface forcings with a timescale of one hour or less (Stull, 1988). The structure and evolution of the ABL are of great importance to military applications. Of particular interest is the height of the boundary layer, (BLH, or Z_i), which is a key input parameter to the atmospheric transport and dispersion (ATD) models. Since the daytime boundary layer (BL) over land is generally well mixed, the BL is sometimes referred to as the mixed layer and Z_i is hence referred to as the mixing height. The BL thickness is quite variable in time and space, ranging from hundreds of meters to a few kilometers. The top of the ABL is capped by a layer of stable thermal stratification, which is commonly known as the capping inversion. The interface between the capping inversion and the BL is called the entrainment zone (EZ) which separates the BL from the free atmosphere (FA). The daytime overland BL is often capped by a well-defined inversion, which rises each morning in response to the growing convective activity below and fades or recedes as the surface heating tapers off near sunset. At night or over the ocean when the ABL has stable stratification, the top of the BL may not be well defined.

Over land surfaces, the BL has a well-defined structure that evolves with the diurnal cycle (see Figure 1). The three major components of the structure are the surface layer (SL), the mixed layer (ML), the residual layer (RL), and the stable boundary layer (SBL). The focus of this thesis is on defining the ML top, and more specifically Z_i. The SL is the region at the bottom of the boundary layer when turbulent fluxes and stress vary by less than 10% of their total magnitude. The ML makes up approximately 35-80% of the convective boundary layer (CBL). This layer is characterized by a nearly constant specific humidity and virtual potential temperature profile with height. The ML is the layer that contains large thermals and sometimes is complicated by the presence of horizontal roll vortices and mesoscale cellular convective activities. The SBL develops

1

after sunrise near the surface while the remaining daytime ML becomes the residual layer when the surface forcing is cutoff after the development of the surface-based stable layer.
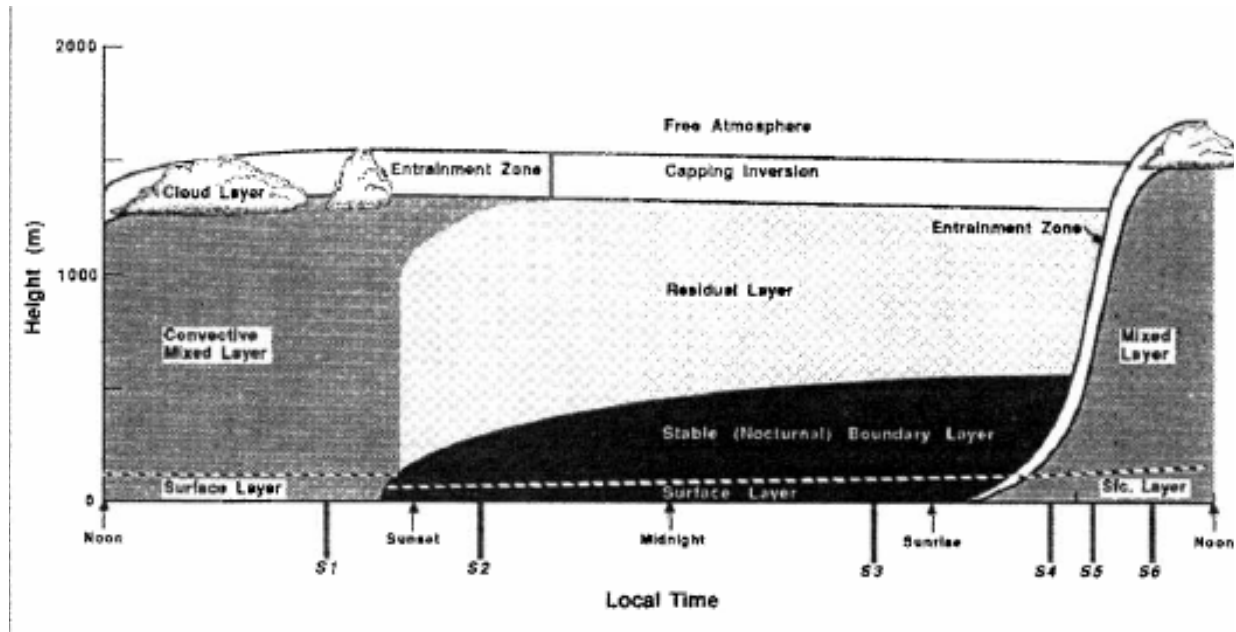
Figure 1.   A typical diurnal evolution of the atmospheric boundary layer over a 24-hour period (From: Stull 1988).

B.   BOUNDARY LAYER HEIGHT IN VARIOUS APPLICATIONS

The BL is very important because this is where people spend most of their lives. Daily weather forecasts of fog, dew, frost, and temperatures are essentially boundary layer forecasts. Pollution is trapped in the boundary layer, and turbulence is prevalent as well. To the US Department of Defense (DoD), the boundary layer parameters are important when it comes to dispersion and transport modeling of chemicals. The Department of Defense (DoD) and other government agencies use several dispersion models including the Second-order Closure Integrated Gaussian Puff model (SCIPUFF), the DoD certified Lagrangian Gaussian D2-Puff model (D2PUFF), Hazard Prediction and Assessment Capability (HPAC), and various Gaussian plume models. These dispersion models are used in the detection of Chemical, Biological, Radiological, Nuclear, and

2

High Yield Explosive (CBRNE) hazards as well as in air pollution hazard estimates. Uncertainties in the meteorological input account for more than half of the total uncertainty in predicting the observed one-hour ground level concentrations using a complex second order closure plume model. Among all the meteorological input, the BL height is a critical variable to dispersion modeling as errors in BL height result in significant errors in forecast concentrations. Therefore, there is a need to quantify the uncertainties in BL height as input to dispersion models (Rao, 2004).

Boundary layer height is also an important scaling length for the normalization of boundary layer parameters such as fluxes and variance including vertical gradients of wind, potential temperature, and moisture. In addition, BL height is also involved in some of the boundary layer parameterizations in mesoscale models where turbulent kinetic (TKE) schemes depends heavily on the parameterization of turbulence length scales to describe eddy diffusion coefficients for momentum and scalar mixing (e.g., Therry and Lacarrere, 1983).

C.   BOUNDARY LAYER HEIGHT FROM MODELS

Boundary layer height is not a predicted quantity in mesoscale models. In general, it is diagnosed based on the bulk Richardson number. BLH is not a routine measurement from weather stations, either. Frequently, particularly when used as input to dispersion models, it is derived from mesoscale forecast models. However, few studies have focused on evaluation of the BLH from mesoscale models. Angevine and Mitchell (2001) conducted an evaluation of the National Centers for Atmospheric Predictions (NCEP) mesoscale Eta model for the convective boundary layer. Their studies indicated that the models were fairly accurate in their depiction of the mixing height. Other previous research has identified substantial errors in the BLH from mesoscale models. Eleuterio et al. (2004), e.g., examined BL height from the Navy's Coupled Ocean and Atmospheric Prediction System (COAMPS) in comparison with aircraft measurements in cases of stratocumulus-topped boundary layers in the coastal California region. They found that the BLH from COAMPS was in general underestimated by 100 m. Under certain cases, the BLH was significantly lower than the

observations by several hundred meters. Clearly, a better evaluation of the BLH generated from the mesoscale models is needed for various atmospheric conditions.

D.   BOUNDARY LAYER HEIGHT FROM OBSERVATIONS

Boundary layer height can be obtained from observations through a variety of measurement variables. Using a research aircraft equipped with turbulence measurement capability, the local boundary layer top can be identified with accuracy of about 10 m or less when the aircraft penetrates through the boundary layer top and identifies the turbulent layer (Wang et al, 1999). With the ground-based measurements, the most straight-forward method is through the analysis of the vertical variations of temperature, humidity, wind (Norris, 1998; Johansson et al, 2001, Zeng et al., 2004) and even the balloon ascent/descent speed of the routine rawinsonde (Johansson and Bergstro 2005). Boundary layer height defined from a rawinsonde sounding is generally taken as the true observed BLH although variability may result from different criteria of the temperature gradient used to define the boundary layer top and that the local boundary layer height from a single balloon sounding is likely different from the mean boundary layer height .

In recent years, in addition to radiosonde data, remote sensing data from sodar (Vogelezang and Holtslag 1996), lidar (Drobinski et al. 1998) and wind profiler/RASS systems have been used extensively to detect boundary layer height from continuous measurements of the radar reflectivity at different wavelength. Unlike the BLH from aircraft or rawinsonde, the radar detected BLH are continuous in time for a long period. Cohn and Angevine (2000) shows, using their results from the '96 Flatland experiment that profiles from single rawinsonde ascents give only rough estimates of mixing height and may be at times completely misleading for the EZ depth. They used rawinsonde derived BLH to compare with that from the profiler data and found that the discrepancies can be significant if the rawinsonde ascends in a thermal rather than between thermals. For this reason, radar wind profilers are considered dependable means to estimate the height of the mixed layer. On the other hand, since the vertical resolution of the profiler measurements is relatively coarse, on the order of 60 to 100 m, and there exists different algorithms for deriving BLH from the profiler measurements, the accuracy of the BLH

4

from profilers needs to be examined as well. Nevertheless, the abundance of data from the profiler/RASS system makes it possible for systematic evaluation of BLH from mesoscale models under various conditions.

E.   SCOPE OF RESEARCH

The objective of this research is to use continuous profiler/Radio Acoustic Sounding System (RASS) measurements to examine the uncertainty of the BLH from mesoscale models. The main focus is on the daytime CBL over land.   The boundary layer height was detected using two methods, which will be described in more detail in Chapter IV, and was validated against those from the rawinsonde soundings. In Chapter II, the general characteristics of the ABL are discussed, including turbulence and physical processes that modify turbulent kinetic energy (TKE).   Chapter III describes the measurements used in this thesis from the Marine Atmosphere Measurement Lab (MAML) at the Naval Postgraduate School (NPS) and Miramar measurement site (MMR). Chapter IV discusses the BLH detection schemes using the profiler/RASS measurements and evaluates the results of BLH using the NPS detection schemes in comparison with those from rawinsonde measurements. Main results will be given in Chapter V, where the BLH from the Weather Research and Forecasting (WRF) model will be compared to the BLH from profiler/RASS system. Testing of an alternative method to diagnose BLH from WRF is also discussed in Chapter V. Finally, Chapter VI will give a summary, conclusions, and recommendations from this research.   The research subject directly supports recommendations brought forth by the Joint Action Group on Federal Research and Development dealing with atmospheric transport and diffusion.

THIS PAGE INTENTIONALLY LEFT BLANK

II.   BOUNDARY LAYER AND MODEL BACKGROUND DISCUSSION

A.   BOUNDARY LAYER PHYSICAL PROCESSES

The atmospheric boundary layer is characterized by the presence of turbulence generated by the mean wind shear or by buoyancy flux. Usually, the largest wind shear is found near the surface although moderate wind shear also present at the boundary layer top. Buoyancy flux contributes directly to the generation/consumption. On a sunny day overland, surface buoyancy flux is a major source of turbulence which results in the daytime convective boundary layers. Turbulence generated by buoyancy flux is also seen in the cloud-topped boundary layers where positive buoyancy flux at the upper boundary layer is a result of radiative cooling at the cloud top. In the stable boundary layer, wind shear becomes the sole source of turbulence as the negative buoyancy flux consumes turbulent kinetic energy. The generation of turbulent kinetic energy (TKE) is depicted in Eq. (1) below for horizontally homogeneous conditions.

$$\frac{\partial \overline{e}}{\partial t} = \frac{g}{\overline{\theta_v}} \overline{w'\theta_v'} - \overline{u'w'}\frac{\partial \overline{U}}{\partial z} - \overline{v'w'}\frac{\partial \overline{V}}{\partial z} - \frac{\partial \overline{w'e}}{\partial z} - \frac{1}{\overline{\rho}}\frac{\partial \overline{w'p'}}{\partial z} - \varepsilon \tag{1}$$

where e represents TKE, ε is the turbulent dissipation rate, θ_v is the virtual potential temperature, u, v, w represent the perturbation wind components, while $\overline{U}, \overline{V}$ are the mean horizontal wind components. The first term on the right-hand-side (RHS) of Eq.(1) is the buoyancy production/consumption term of TKE, the second and third terms on the RHS represent TKE tendency caused by mean wind shear, the fourth and fifth terms represent turbulent transport and pressure transport, respectively. In a clear convective boundary layer, turbulence is generated near the surface by mainly buoyancy flux at the surface (and sometimes together with wind shear) and is transport upward to the upper mixed layer through turbulent transport (Deardorff 1980). Figure 2 illustrates the TKE balance in a typical clear convection boundary layer as discussed above.
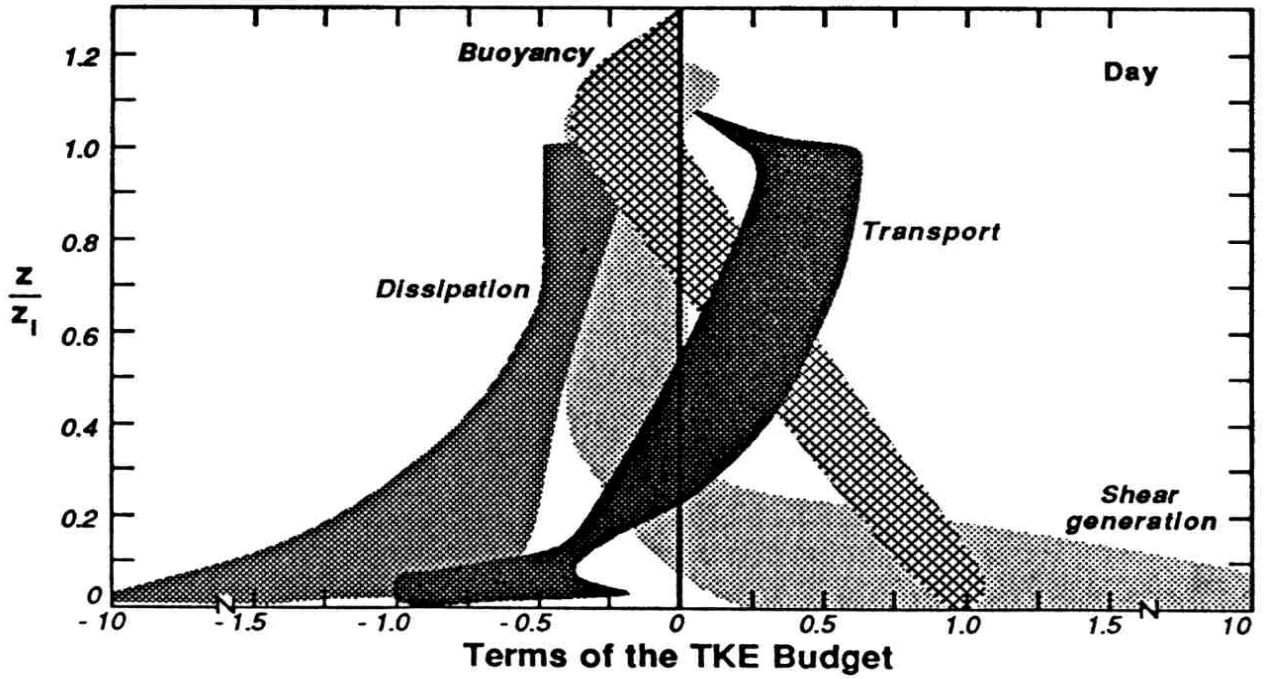
Figure 2.   Normalized terms in the turbulence kinetic energy equation. The shaded areas indicate ranges of values. All terms are divided by w^3_*/z_i, which is on the order of $6\times10^{-3}\,\mathrm{m^2 s^{-3}}$. (From: Stull)

In response to surface and upper air forcing, boundary layer mean profiles evolves accordingly.   Figure 3 shows several examples of the virtual potential temperature profiles during a diurnal cycle starting at around 1600 local time. The corresponding time of the day for each panel is indicated in Figure 1. The presence of the mixed layer is seen during daytime (S1) which is capped by a strong temperature inversion. Very often, a significant decrease in water vapor also exists across the inversion when the difference in specific humidity between the mixed layer and the free atmosphere is on the order of several to 10 g kg^{-1}. The clear convective boundary layer will be the focus of this study when the BLH from WRF are compared to those from observations.
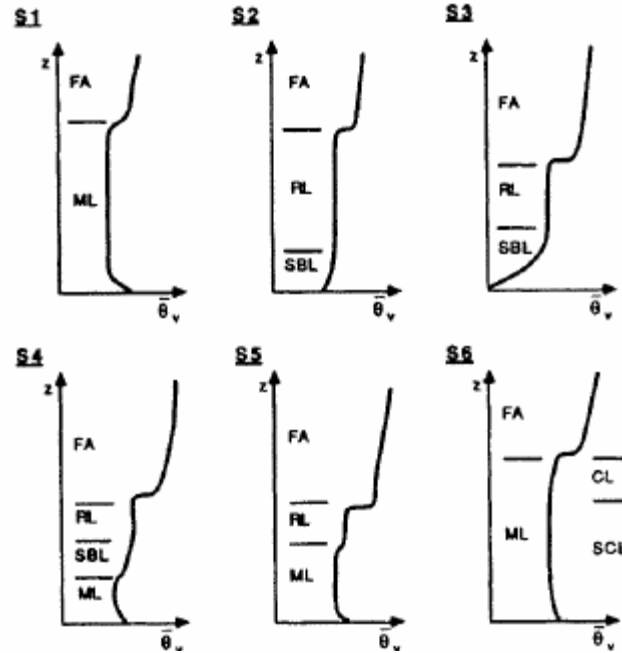
Figure 3.   Profiles of mean virtual potential temperature showing the boundary evolution during a diurnal cycle starting at about 1600 local time. S1-S6 identify each sounding with an associated launch time. (From: Stull)

B.   ENTRAINMENT ZONE AND CHARACTERISTICS OF THE MIXED LAYER TOP

The entrainment zone (EZ) is the region of statically stable air at the top of the ML, where there is entrainment of FA air downward and overshooting thermals upward. In case of free convection, buoyant thermals from the surface layer gain momentum as they rise through the mixed layer. Upon reaching the warmer FA, they find themselves negatively buoyant, but overshoot a short distance because of their momentum, which is called "penetrative convection" (Stull, 1988).   This process results in the undulating structure as depicted in Figure 4 below.   The EZ can be up to 40% of the depth of the ML. The top of the EZ is defined as the altitude of the highest thermal in the region.

9
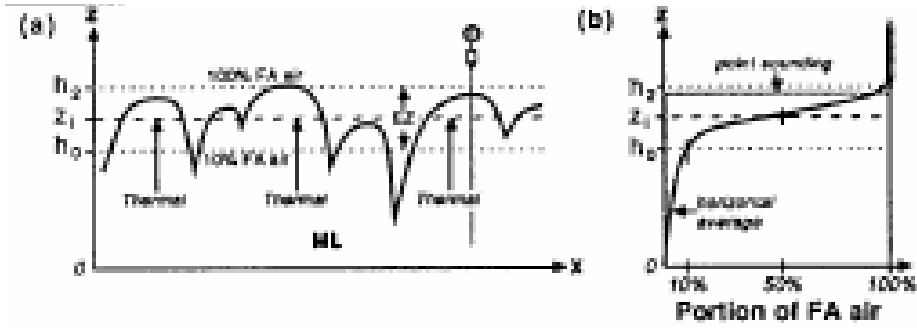
Figure 4.   The EZ can be defined in terms of the fraction of FA air. (a) Overshooting thermals cause rawinsonde sounding to indicate improper values of zi. Solid line is the local ML top, while the dashed line is the average ML top, zi. (b) Variation of fraction of FA air with height in the EZ as measured by horizontal averages (solid line) and a point sounding (dotted line) (From: Stull).

Defining the bottom of the EZ is more difficult because there is no sharp demarcation. One approach is to take the altitude where about 5-10% of the air on the horizontal plane has FA characteristics (Deardorff, et al., 1980; Wilde, et al., 1985). Since the EZ is also statically stable, the buoyancy flux is normally negative in the EZ. Hence, an alternative method to define the bottom of the EZ is to find the level where the buoyancy flux becomes negative.

The average ML depth, or the boundary layer height, is defined as the altitude where 50% of the air has FA characteristics on a horizontal average as illustrated in Figure 4. Thus, the boundary layer height is a statistical quantity representing an ensemble average of the 50% mixing level. Unfortunately, measurements of the mixing fraction and its spatial variation are never truly available even with a research aircraft flying near the top of the mixed layer. With in-situ measurements, most likely we have balloon soundings, dropsondes, or aircraft slant-path penetrations that go through the mixed layer top at a specific location. These in-situ penetrations are point measurements. Boundary layer heights from these individual penetrations may differ from the average as illustrated in Figure 4. Obtaining averages of the mixed layer height from multiple penetrations at the same time is thus highly desirable but is rarely available. From this perspective, BLH from remote sensors, which will be discussed later, is advantageous.

10

C. THE STABLE BOUNDARY LAYER

The stable boundary layer (SBL) is one of the most difficult problems in boundary layer meteorology. The typical depth of the SBL is 100-500 m. Because it is often observed at nighttime overland, it is also called the nocturnal boundary layer in that situation although SBL is observed also during the day and in marine environments. The following figure depicts typical profiles of mean absolute temperature, mean potential temperature, mean wind speed, and mean specific humidity.
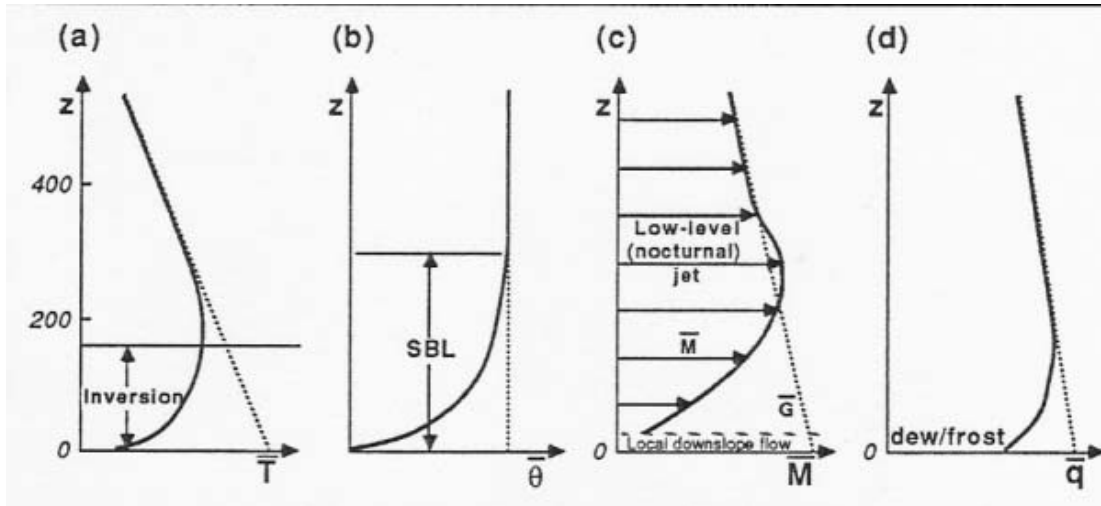
Figure 5.   Typical SBL profiles of mean (a) absolute temperature, (b) potential temperature, (c) wind speed, and (d) specific humidity. (From: Stull)

Defining the SBL height can be a difficult process since the height can be defined from different criteria. For instance, the top of the SBL could be the height where the lapse rate is adiabatic, or it could be the location of the nocturnal jet level. SBL's were not investigated in this study, however further investigation into model comparison and SBL height should be done to understand the complete strengths and weaknesses of the WRF model when detecting BLH at any hour of the day.

11

D.   PBL SCHEMES AND BOUNDARY LAYER HEIGHT IN WEATHER RESEARCH AND FORECASTING (WRF) MODEL

1.   General Information

The Weather Research and Forecasting (WRF) Model is a next-generation mesoscale numerical weather prediction system designed to serve both operational forecasting and atmospheric research needs. It features multiple dynamical cores, a 3-dimensional variational (3DVAR) data assimilation system, and a software architecture allowing for computational parallelism and system extensibility. WRF is suitable for a broad spectrum of applications across scales ranging from meters to thousands of kilometers.

The effort to develop WRF has been a collaborative partnership, principally among the National Center for Atmospheric Research (NCAR), the National Oceanic and Atmospheric Administration (NOAA), the National Centers for Environmental Prediction (NCEP) and the Forecast Systems Laboratory (FSL), the Air Force Weather Agency (AFWA), the Naval Research Laboratory, Oklahoma University, and the Federal Aviation Administration (FAA). WRF allows researchers the ability to conduct simulations reflecting either real data or idealized configurations. WRF is currently in operational use at NCEP. The Air Force has also recently starting running the WRF model in the early summer of 2007. Currently, the model is run operationally over areas overseas but is not yet being run over the CONUS (Continental United States). The Air Force will eventually transition fully from MM5 to WRF for operational use over the CONUS.

2.   Planetary Boundary Layer Schemes in WRF

The PBL scheme in a mesoscale model is responsible for vertical sub-grid-scale fluxes due to eddy transports in the whole atmospheric column, not just the BL. Thus, when a PBL scheme is activated, explicit vertical diffusion is de-activated with the assumption that the PBL scheme will handle this process.

The PBL schemes provide atmospheric tendencies of temperature, moisture (including clouds), and horizontal momentum in the entire atmospheric column. Most

PBL schemes consider dry mixing, but can also include saturation effects in the vertical stability that determines the mixing. The schemes are one-dimensional, and assume that there is a clear scale separation between sub-grid eddies and resolved eddies. This assumption will become less clear at grid sizes below a few hundred meters, where BL eddies may start to be resolved, and in these situations, the scheme should be replaced by a fully three-dimensional local sub-grid turbulence scheme such as the TKE diffusion scheme. (NCAR, 2006)

The three choices of PBL schemes are summarized in Table 1. The Medium Range Forecast Model (MRF) scheme is described in Hong and Pan (1996). This PBL scheme employs a so-called counter-gradient flux for heat and moisture in unstable conditions. It uses enhanced vertical flux coefficients in the PBL, and the PBL height is determined from a critical bulk Richardson number. It handles vertical diffusion with an implicit local scheme, and it is based on local R_i in the FA. (NCAR, 2006)

Table 1.   The basic features of the PBL schemes in Advanced Research Weather (ARW) (From: NCAR Tech Note)

Scheme	Unstable PBL Mixing	Entrainment treatment	PBL Top
MRF	K profile + countergradient term	part of PBL mixing	from critical bulk R_i
YSU	K profile + countergradient term	explicit term	from buoyancy profile
MYJ	K from prognostic TKE	part of PBL mixing	from TKE

The Yonsei University (YSU) PBL scheme is the next generation of the MRF PBL, also using the countergradient terms to represent fluxes due to non-local gradients. This adds to the MRF PBL an explicit treatment of the entrainment layer at the PBL top. The entrainment is made proportional to the surface buoyancy flux in line with results from studies with large-eddy models. The PBL top is defined using a critical bulk Richardson number of zero (compared to 0.5 in the MRF PBL), and is therefore effectively only dependent on the buoyancy profile which, in general, lowers the calculated PBL top compared to MRF. (NCAR, 2006)

The Mellor-Yamada-Janjic (MYJ) PBL parameterization (Janjic, 1990, 1996, 2002) represents a nonsingular implementation of the Mellor-Yamada Level 2.5 turbulence closure model (Mellor and Yamada, 1982) through the full range of atmospheric turbulent regimes. In this implementation, an upper limit is imposed on the master length scale. This upper limit depends on the TKE as well as the buoyancy and shear of the driving flow. In the unstable range, the functional form of the upper limit is derived from the requirement that the TKE production in the case of growing turbulence. In the stable range, the upper limit is derived from the requirement that the ratio of the variance of the vertical velocity deviation and TKE cannot be smaller than that corresponding to the regime of vanishing turbulence. The TKE production/dissipation differential equation is solved iteratively.

The boundary layer height (BLH) in most of the PBL schemes in WRF are defined at the lowest model level when the Bulk Richardson number exceeds a critical value. The local bulk Richardson number (Ri_b) is defined as:

$$R_{ib} = \frac{(\frac{g}{\theta_v})\Delta\overline{\theta}_v\Delta z}{(\Delta\overline{U})^2 + (\Delta\overline{V})^2}$$

Where $\Delta z, \Delta\overline{\theta}_v$, $\Delta\overline{U}$, and $\Delta\overline{V}$ are thickness and change of potential temperature and horizontal wind components across the layer, respectively. Theoretically, one can use the gradient Richardson number to determine the dynamic stability of the flow in comparison with the Critical Richardson number (with a value of 0.25). When this criterion is applied to the model generated flow field, the bulk Richardson number is used instead because finite differencing is used in place of the vertical gradient. As a result, the critical value used to determine the highest turbulent level may not be the original critical Richardson number.

Based on Hong and Pan (1996) the bulk Richardson number for diagnosing BLH is defined as:

$$h = Rib_{cr}\frac{\theta_{va}|U(h)|^2}{g(\theta_v(h) - \theta_z)}$$

where Rib_{cr} is the critical bulk Richardson number, θ_s and θ_{va} are virtual potential temperatures near the model surface and at the lowest sigma level, respectively. $\theta_v(h)$ is the virtual potential temperature and $U(h)$ is the horizontal wind speed at the boundary layer top (h).

THIS PAGE INTENTIONALLY LEFT BLANK

III: INSTRUMENTATION AND DATA

The major instruments used for this study is the 915-MHz wind profiler and the Radio Acoustic Sounder System (RASS).   We also used measurements from the rawinsonde system to identify the boundary layer height.   These instruments will be discussed in this chapter.

A.   BASICS OF THE RADAR WIND PROFILER AND RADIO ACOUSTIC SOUNDER SYSTEM (RASS)

The 915-MHz boundary layer wind profiler (Figure 6) was developed at the National Oceanic and Atmospheric Administration (NOAA) Aeronomy Laboratory.   The systems are sensitive Doppler radars, designed to respond to refractive index fluctuations in clear air.   The 915-MHz radar has a 32.8-cm wavelength. This relatively short wavelength allows a relatively small antenna size.   The aperture of the antenna, which is controlled largely by practical considerations, determines two other characteristics of the antenna, the beam width and the antenna gain. The beam width is inversely proportional to the aperture. The antenna gain is directly proportional to the aperture. (Helsinki, 2008)

Figure 6.   NOAA 915MHz boundary layer wind profiler and RASS. (From: Argonne National Laboratory)

The RASS works through the properties of sound wave propagation. The RASS system, usually composed of four acoustic sources (one on each side of the profiler antenna) transmits an acoustic wave directed vertically. The profiler uses the acoustic wave as a target, receiving and processing the resulting backscatter and effectively measuring the speed of sound propagation. The profiler can compute virtual temperature (T_v) profiles because the speed of sound is affected by air temperature and humidity. Raw temperature data are stored in the moment and spectral data files, but separated from wind data. Variations in speed of sound can be converted to a virtual potential temperature profile of the atmosphere. Figure 7 shows an example of the profiler/RASS measured wind and temperature profiles. The virtual potential temperature is estimated from the measured virtual temperature at each measurement level.
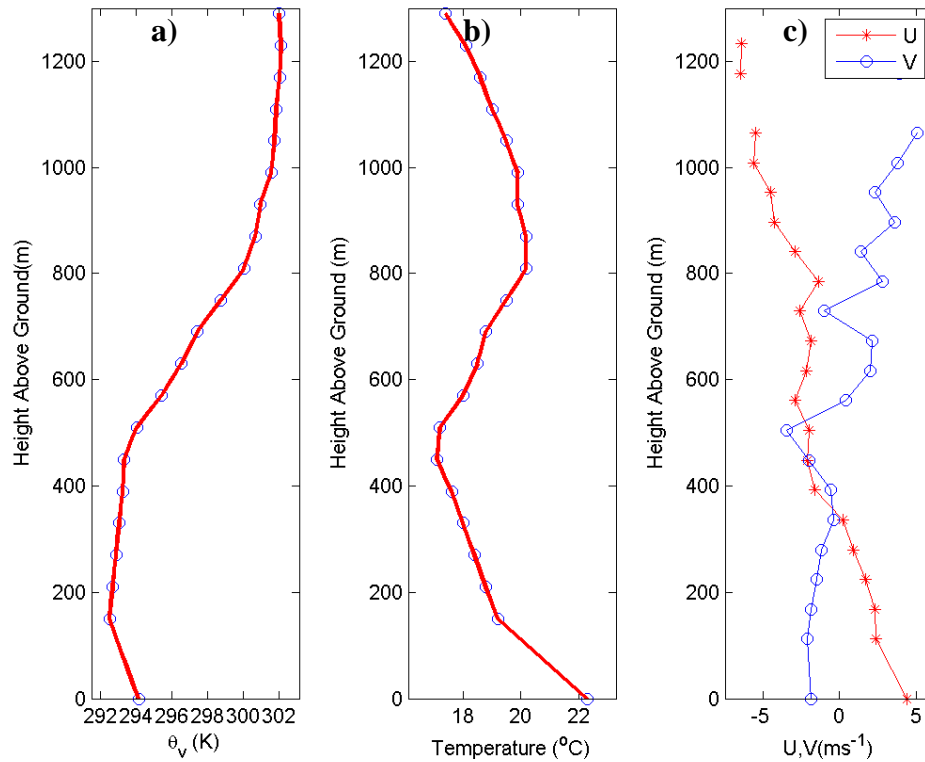
Figure 7. An example of the vertical profiles of a) potential temperature (converted from the virtual temperature measurement), b) air temperature, and c) horizontal wind components from profiler/RASS system. The measurements were made on 22 Aug 2002 at 0900 PST from the NPS Marine Atmospheric Measurement Lab at Fort Ord.

18

B.   ATMOSPHERIC EFFECTS ON PROFILER PERFORMANCE

The range performance of all profilers depends on atmospheric conditions, which can change dramatically and rapidly. The conditions that affect profiler performance include temperature, humidity, turbulence intensity, and precipitation.

Tracking refractive irregularities, which are carried by the wind, reveals information about the wind itself. The profiler computes height by using the time interval between transmission of the pulse and reception of the return signal. However, wind speed and direction are determined based on the Doppler principle. A backscattered wave will shift in frequency because of the motion of the target relative to the observer. A frequency higher than the transmitted frequency indicates that the wind is moving towards the profiler. A frequency lower than the transmitted frequency indicates the wind is moving away from the profiler. The profiler detects these small shifts in the frequency of the backscatter and translates them into wind velocity data.

The amount of moisture in the atmosphere affects the height range performance of the profiler. Generally, the more moisture, the better the profiler works for winds because of the large variations of refractive index. Marine environments make good profiler sites because of the moisture usually prevalent in those regions. The RASS benefits from high humidity levels also. When the atmosphere contains more moisture, there is less attenuation (decrease) of the acoustic signal with range.

The amount of turbulence in the atmosphere also affects the range performance of the profiler. The more turbulence in the atmosphere, particularly turbulence on a scale of one-half the profiler wavelength, the better the profiler works. Turbulence is also beneficial to RASS operation. Turbulence helps distribute the acoustic wavefront, helping increase the range in the presence of winds. The wavelength of the acoustic signal must be half that of the radar signal in order to measure the velocity of propagation of the acoustic signal.

Most types of precipitation such as rain, snow, and hail can affect the performance of the profiler. When precipitation moves in a direction that is different from

the air around it, the vertical beam measures the movement of the hydrometeors rather than the vertical component of the wind. However, if the precipitation is carried with the wind, then the horizontal winds might still be measured because the particle velocity in the off-zenith beam can be corrected with the vertical beam measurement, assuming spatial homogeneity. For RASS, virtual temperature measurements are usually poor quality during precipitation. During precipitation, if the hydrometeor fall velocity is measured and it differs from the vertical wind velocity, the resulting virtual temperature measurements will be incorrect.

Ground clutter most often affects the quality of data in the lower range gates. High winds can cause clutter signals from objects such as trees and power lines to exhibit sufficient Doppler velocity width that the profiler's ability to screen out this clutter is overwhelmed. Choosing sites with minimal ground clutter will improve the range and data quality of the profiler. High winds can adversely effect the RASS virtual temperature measurement in two ways. Increased ground clutter can create incorrect vertical velocity values used for temperature correction. High winds may also reduce the range of measurement of RASS by displacing the acoustic signal away from the radar beam.

Temperature has more of an effect on RASS than on the profiler's wind measurement. Acoustic attenuation varies as a function of temperature, humidity, and pressure. Cold dry air exhibits highest attenuation, which can exceed -40 dB per kilometer. Very moist or warm air propagates acoustic signals better, resulting in improved range for virtual temperature measurement. (Helsinki, 2008)

C.   RAWINSONDE

Rawinsonde is the most common upper-level in situ measurements in the field of meteorology. During their ascent, the balloon-borne instruments radio back to the ground-based receiving station with a nearly continuous stream of information until the balloon bursts at approximately 10 mb. The rawinsonde system provides measurements of air temperature, pressure, moisture, and wind information at various levels in the atmosphere.

The drifting of a radiosonde provides an indirect measure of the wind speed and direction at various levels throughout the troposphere where the location of the balloon at each time is tracked through GPS or previously Loran-C systems.

The rawinsonde data from the NOAA weather stations are normally encoded and transmitted over a communications network to NCEP. At this center, the data can be processed for analysis on upper air charts and for use in numerical weather prediction models. To accomplish this task, all upper air stations are to report RAOB data for certain mandatory pressure levels. To speed the transmission process, the RAOB operator encodes only the temperature and dewpoint data for significant pressure levels along with the mandatory pressure levels. The significant pressure levels are those points ascertained from the plotted sounding where a significant change in the temperature and or dewpoint profile is detected (Hopkins, 1996).

D.   DATA USED FOR THIS STUDY

The data we used for this thesis research were obtained from two measurement sites with the same profiler/RASS systems. The Meteorology Department of the Naval Postgraduate School maintains the Marine Atmospheric Measurement Lab (MAML) at Fort Ord, CA located at (36.69 N, 121.76W) at 51 m elevation above sea level (ASL) and is situated approximately five km inland from the coastline. The instruments maintained at the site include a profiler/RASS sounding system, surface measurements, and a laser ceilometer. The profiler/RASS system operates continuously with measurements every 30 minutes. Surface measurements were recorded as two-minute averages. Data from the summer months between 2000 and 2003 at this location were used to develop and validate the BLH detection scheme.   Another location, Miramar, CA (MMR), which also has a profiler/RASS system as well as rawinsonde data was investigated for comparison and verification purposes. Data from this site was collected from the summer months of 2007. The MMR site is located approximately eight miles inland in southern California outside of San Diego. It is co-located with the Doppler wind profiler used by NOAA and the military.

The rawinsonde data from the station at MMR is used to evaluate the BLH measurements from the profiler/RASS system. The rawinsonde measurements at MMR were made twice daily at 00Z and 12Z and the data were archived at the University of Wyoming at the Department of Atmospheric Sciences and was downloaded from http://weather.uwyo.edu/upperair/sounding.html. These soundings were achieved at the significant levels only. For purpose of this study, we have used measurements from July, August, and September in 2006 and 2007. The Miramar-San Diego profiler site operates the 915MHz profiler/RASS system hourly throughout the year. The profiler operates in two modes: the low mode starts the profiling at five minutes past the hour and has a vertical resolution of about 60 m with the first range gate at about 96 m above ground; the high mode profiling starts 1.5 minutes later and has a vertical resolution of about 100 m with the first range gate at about 200 m above ground. The RASS measures the virtual temperature profile at the beginning of each hour with a vertical resolution of 60 m and the first range gate at 90 m.

IV: BOUNDARY LAYER HEIGHT DETECTION FROM OBSERVATIONS

A.   DETECTING BOUNDARY LAYER HEIGHT FROM RAWINSONDE PROFILES

The clear convective boundary layer is often topped by a strong temperature inversion accompanied by significant decrease of water vapor across the inversion as illustrated in Figure 1. This property has been used to identify the local BLH from a single rawinsonde where we define the BLH at the base of the inversion layer. Figure 8 shows an example of the rawinsonde profiles going through the low-level atmosphere measured by the NPS rawinsonde system. The figure uses the original data received at two second intervals. At an ascent rate of several meters per second, the vertical resolution of the balloon sounding is less than 10 m. In Figure 8, the temperature inversion and the sharp decrease of specific humidity at the boundary layer top are apparent. The BLH is defined as the base of the temperature inversion at 550 m.

03060116.CAP
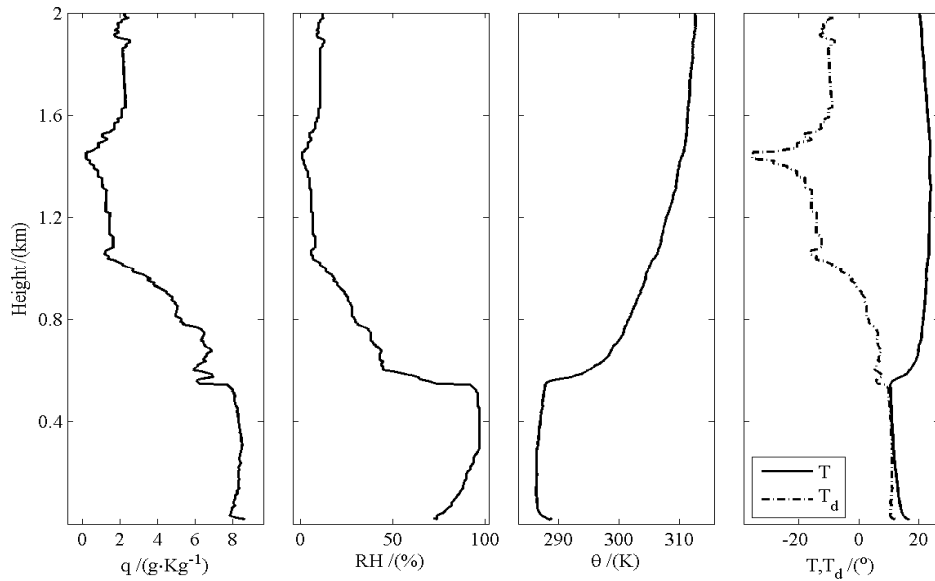
Figure 8.   Vertical profiles of specific humidity, relative humidity (RH), potential temperature (θ), temperature and dewpoint temperature from a rawinsonde ascent off the coast of southern California (32.98N, 118.51W) on June 1, 2003. The BLH is defined as the base of the temperature inversion at about 550 m.

23

Sounding data downloaded from the NOAA data center appear to be different as the data were recorded at the significant levels only. However, the main feature of the sounding profiles should be kept in the selection of significant levels, including the altitude of the inversion layer. An example of the sounding profiles from the MMR site is shown in Figure 9. From this figure, we can identify the BLH at about 640 m.
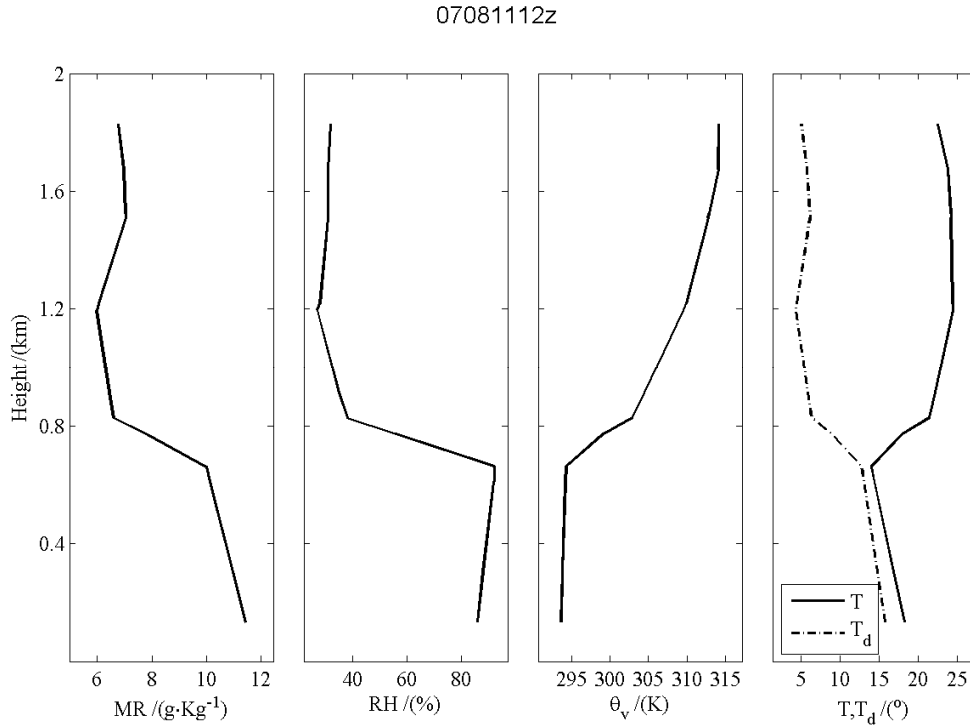
Figure 9. Vertical profiles of specific humidity, relative humidity (RH), potential temperature (θ), temperature and dewpoint temperature from a rawinsonde ascent at the MMR site on August 11, 2007. The BLH is defined as the base of the temperature inversion at about 550 m.

Using the same method, we obtained BLH from six summer months (July, August, and September 2006 and 2007) from the MMR site. These BLH's are used to compare to those derived from the profiler/RASS system to evaluate the remotely-sensed BLH. However, it is important to keep in mind that profiles from single rawinsonde ascents may not be representative of that of the average BLH because the rawinsonde will find a different result if it ascends in a thermal rather than between thermals. For fair comparisons, BLH's from many soundings should be used.

B. DETECTING BOUNDARY LAYER HEIGHT FROM PROFILER/RASS --- PREVIOUS STUDIES

1. Boundary Layer Height and Signal-to-Noise-Ratio Profiles

Measuring the BLH is complex due to the fact that the inversion height is often higher than stationary measurement equipment can reach. Balloon and aircraft soundings have been used but may not be completely representative in the spatial or temporal scales. Therefore acoustic, microwave, and optical techniques have been used and studied to obtain the best estimate of BLH in the atmosphere.

The entrainment in the interfacial layer can create a strong vertical gradient in the temperature and humidity profiles, which causes a maximum in the profile of the refractive index structure parameter C_n^2, resulting in an enhancement of sodar and ultrahigh frequency (UHF) profiler returns. Numerous studies based on numerical modeling and/or experimental data have shown that the vertical profiles of the refractive index structure parameter C_n^2 have an pronounced maximum near the base of the capping inversion layer or where the humidity gradient is large (e.g., Burk 1980;Wyngaard and LeMone 1980;Angevine et al., 1994). This relationship is based on the assumptions that refractive index irregularities are in equilibrium with steady-state turbulence and that the radar wavelength lies in the inertial subrange of the turbulence (Ottersten 1969). Since the range-corrected Signal-to-Noise-Ratio (SNR) of the profiling radar is proportional to the refractive index structure parameter, C_n^2, in clear air (White et al. 1991), defining the BLH from the profilers thus becomes an issue of detecting the level of maximum SNR.

A maximum value in backscattered intensity profiles can be also found in clouds because of the enhancement of reflectivity by strong turbulent mixing within the cloud and entrainment mixing near cloud boundaries (Angevine et al., 1994). In addition, since the residual layer from the previous day is also capped by a thin layer of temperature inversion and moisture decrease (Figure 3), a C_n^2 maximum may also observed at the top of the residual layer. Other factors that may result in local peak of the SNR from the profilers include precipitation and biological targets such as insects and birds (Angevine

25

et al., 1994).   Because of these complexities, various methods aimed at identify the maximum SNR corresponding to the BLH has been studied in the past.

2.   Boundary Layer Height Detection Method Based on Signal-to-Noise-Ratio

The boundary-layer profiler can provide continuous measurements of CBL height with very good time resolution (30 minutes or less) and good height resolution (60-100 m). These measurements were pioneered by White et al. (1991a,b) and was later described in White (1993).   White (1993) simply assigns the CBL height as the level of C_n^2 or SNR maximum in an instantaneous vertical profile. It can provide good time resolution of the estimated CBL height since it estimates the height from the SNR maximum of a single profile. However it , may erroneously detect SNR peaks due to other complicating factors such as a cloud layer or the residual layer top.

Angevine et al. (1994) proposed a median filtering method that is based on an increase in backscatter intensity in the same way as the maximum backscattered intensity method. However, a median filter is used to remove C_n^2 peaks from the enhancement of reflectivity by clouds, stable residual layer, precipitation, and biological targets such as insects and birds. Angevine et al. (1994) suggested two algorithms to find CBL height. In the first, a C_n^2 peak in each profile is selected and then the median value of the heights at which the peaks occur during the considered period is determined to be the CBL height. The other is that after taking the median value of the C_n^2 values at each range gate during the considered period, the height that has the peak value in the median C_n^2 profile is determined as the CBL height. The first method was actually used in Angevine et al (1994). With this method, hourly values of boundary layer height for each profiler can be obtained.   This same method was applied to measurements from the Flatland'96 experiment where the profiler BLH was compared to the radiosonde BLH. Overall, they showed close agreement with a slight bias towards a higher measurement from the profiler (see Figure 10).

26
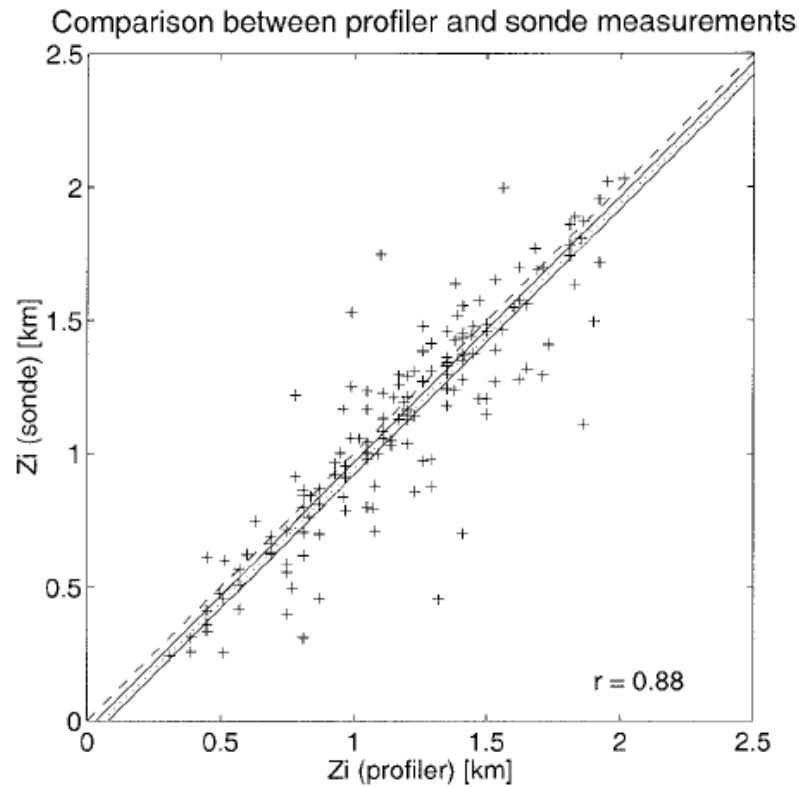
Figure 10.   BLH as determined by radiosonde compared to profiler peak reflectivity. The mean zi from the profiler is 1181m, the mean zi from the radiosonde is 1125m, and the correlation coefficient is .88 from 150 points. The dashed line represents perfect correlation (one-to-one), the dotted line shows the mean difference, and the two solid lines are at the mean difference plus and minus the standard deviation of the mean difference. (From Grimsdell and Angevine, 1998)
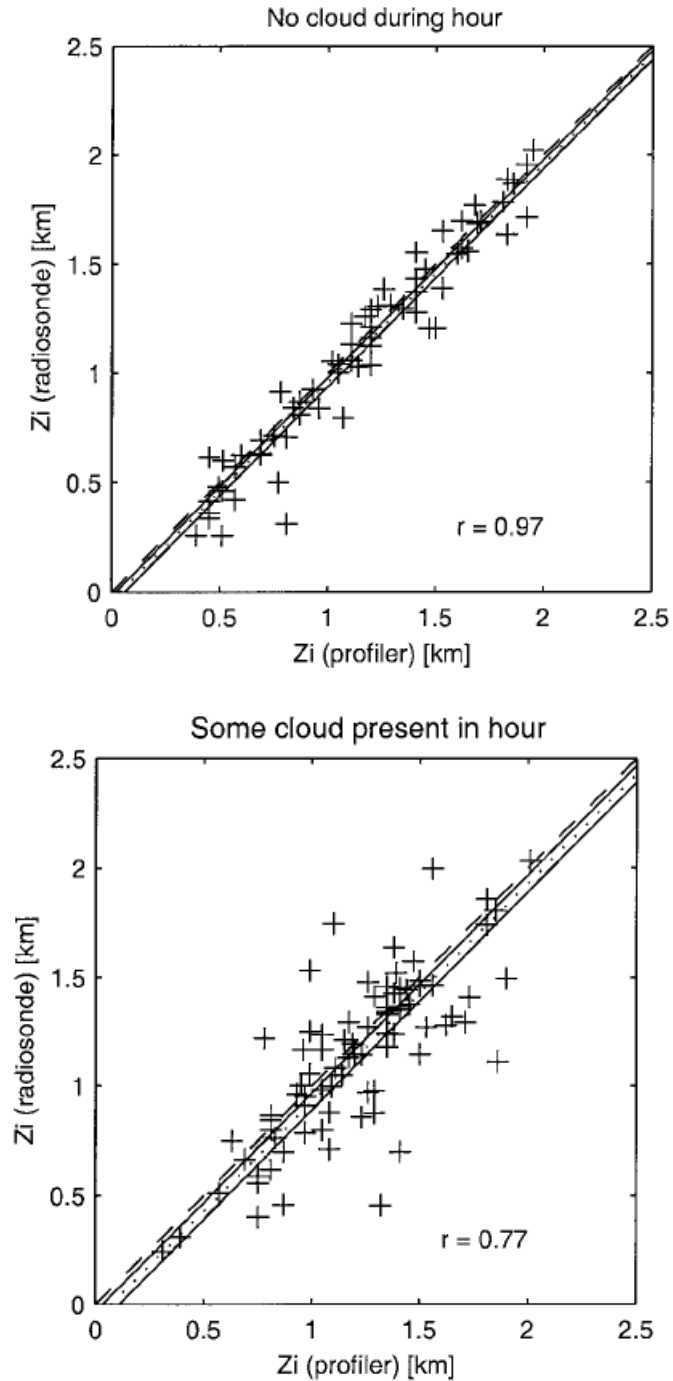
Figure 11.   Radiosonde zi and profiler zi stratified by the presence of cloud during the hour. For clear conditions, the mean profiler zi is 1151m and the mean radiosonde zi is 1110 m. The correlation coefficient is .97 for 67 points. For cloudy conditions, the mean profiler zi is 1207m and the mean radiosonde zi is 1136m. The correlation coefficient is .77 for 83 points. (From Grimsdell and Angevine, 1998)

Grimsdell and Angevine (1998) examined the effects of scattered cumulus on the detection of BLH using the method proposed by Angevine et al. (1994). Figure 11 uses the same data as in Figure 10, except that the data were separated into cloud free and cloudy condition with a mean cloud fraction of 23%. Here we see that reliable estimates of BLH can be made using wind profilers, particularly in the cloud-free conditions. The presence of cloud apparently reduced the correlation between the SNR detected and the rawinsonde derived BLH's.

To deal with the situations where SNR profile has a double peak because of the residual layer and/or cloudy conditions, Heo et al. (2003) examined the behavior of the SNR peaks and proposed a new method by making joint use of peaks and vertical air velocity variance . The capability of their method to estimate the CBL height was compared to those by White (1993) or Angevine et al. (1994) and was found to be advantageous in the presence of double peaks in the SNR profiles.

A relatively new approach in dealing with multiple peaks in the SNR profile is to involve the fuzzy logic techniques (Bianco and Wilczak, 2002). "Fuzzy Logic" was a term coined by Dr. Lotfi Zadeh in 1962 (Sowell). It is basically the way a human brain works, and this can be incorporated into computers and machines. Bianco and Wilczak (2002) used a fuzzy logic approach to reduce or eliminate contamination of the radar moments, and to also include the variance of vertical velocity. Their fuzzy logic method first used a method of applying a fuzzy logic algorithm to the radar spectra to reduce the influence of clutter from a variety of sources, including ground clutter, radio frequency, and point targets. A second fuzzy logic algorithm then used the clutter-suppressed radar SNR measurements to determine the depth of the ML. This algorithm incorporated measures of the peak, gradient, and curvature of hourly median SNR profiles, as well as the profiles of hourly variances of SNR and vertical velocity. When compared to the standard technique for estimating BL depths, the new method was found to be substantially more accurate.

With a similar fuzzy logic approach, Lee at al. (2004) also detected BLH using measurements from 1.29 GHz profiler operated by the Korean Meteorological Administration (KMA). Their algorithm is divided into three steps. First, a fuzzy logic-

based algorithm is applied to the incoming multiple peak data to identify the clear air signal. Second, a consensus algorithm is used on the identified clear air signal to reject outliers and the extract clear air signal as having a poor signal to noise ratio. Third, various quality control algorithms are used to ensure a reliable wind estimate. The resultant BLH's were used to evaluate BLH's from a regional model diagnosed based on bulk Richardson number similar to that described in Hong and Pan (1996). Overall, the wind profiler showed that a ML was better developed in a warm high pressure regime. However, the model ML heights compared to the profiler SNR data showed stable performance but tended to develop the ML too deep and too early, which may be a deficiency in the model's PBL scheme.

C.   THE NPS BOUNDARY LAYER HEIGHT DETECTION METHODS USING PROFILER/RASS MEASUREMENTS

In addition to detecting BLH from rawinsonde profiles, two methods have developed at NPS to detect BLH using measurements from profiler/RASS system. These methods and their results are discussed in this section.

1.   Signal-to-Noise Ratio Method

The algorithm to find the peak altitude corresponding to the BLH is similar to that of Angevine et al. (1994), but is different in specific details. Similar to any other SNR based methods, the first step is to identify the SNR peaks from the range-corrected SNR profiles, which is done through a 'scanning' peak detection routine. The routine basically searches from lower to higher altitudes in the SNR profile to find an altitude for which there are both a lower altitude and a higher altitude with SNR values lower than the value at the examined altitude by at least a predefined threshold. At the altitude with the maximum SNR between the above mentioned lower and higher altitudes (bounds), there is a local maximum (peak) if there is no local minimum (i.e. "negative" peak) between these bounds. The detection predefined threshold is set to be 3 dB and can be changed to test on the sensitivity of the algorithm to this threshold. The BLH height is estimated as a weighted average altitude using SNR between peak bounds as the weight instead of

taking it as simply the altitude of peak SNR. This estimate improves the resolution of BLH detection (provided that the peak is correctly detected) compared to the low resolution of the profiler.

Furthermore, we use the upper and the lower bounds of six previously detected peaks (this number is empirically determined) as a detection 'memory' in order to limit the search of the SNR peak in the current profile within two times the maximum thickness of the inversion (maximum upper minus minimum lower bound of six previous peaks) from the previous (last) BLH detection. If there are RASS measurements available within 10 minutes from profiler data they can used to help in the temporal continuity of BLH detection in case the SNR profile 'memory' is lost (no BLH detected in the last six SNR profiles). For this purpose the gradient method is applied to the RASS virtual potential temperature profile (see next section) in order to find a first estimate of the lower bound (temperature inversion base) of SNR peak from the lowest height where the virtual potential temperature gradient value is larger than a predefined threshold (1 to 2 K/100 m). BLH 'memory' is used to keep the temporal continuity of BLH detection, but this is not always feasible. For example, if a lower inversion develops (e.g. sea breeze front or ground based inversion), then at some time it will be become strong enough that it would be detected by RASS and, thus, there will be a step in the BLH temporal evolution from the detection routine. Thus, in addition to using a BLH 'memory' a quality control is applied at the end of the detection routine using the deviation of BLH values from their moving median with a window length equal to the 'memory' length. Outlier (i.e. wrong detection) BLH values are defined as those values whose deviation from the moving median is more than three times the median of all deviations in each day and are given an error flag. Median averaging is used instead of mean because median it is much less sensitive to the existence of outliers.

Figure 12 is an example of the vertical profile of the SNR from three separate days, where the SNR detected BLH is noted by the dashed red line. We can see that the detected BLHs are at one of the measurement levels corresponding to a local maximum in the SNR profile. Figure 13 shows the time-height contour plots of the SNR from two

10-day periods in July 2007 with the BLH detected from the SNR method. The image shows good agreement between the derived BLH and the height at which the range-corrected SNR is a maximum.
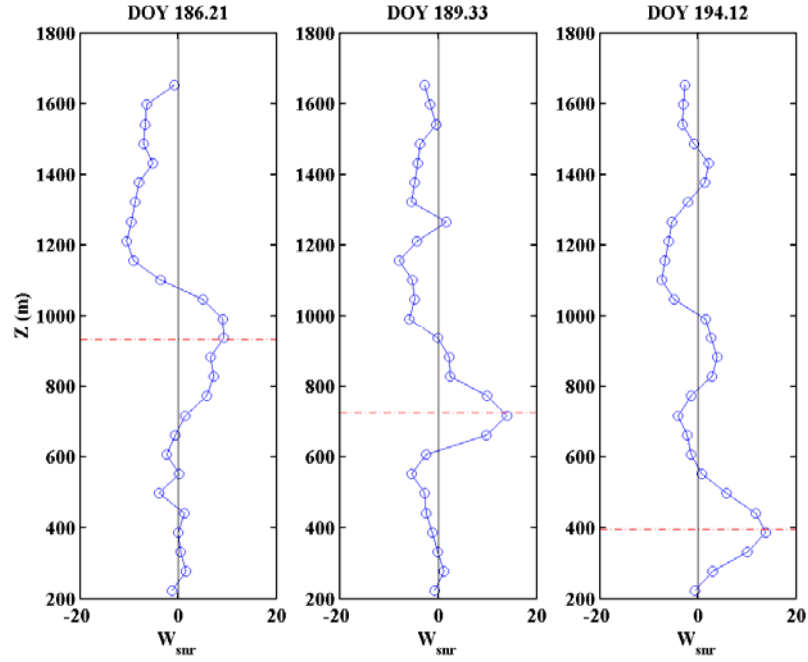
Figure 12.   Examples of SNR profiles from the MMR profiler site during July 2007. The red line denotes the SNR max and is taken as the BLH.
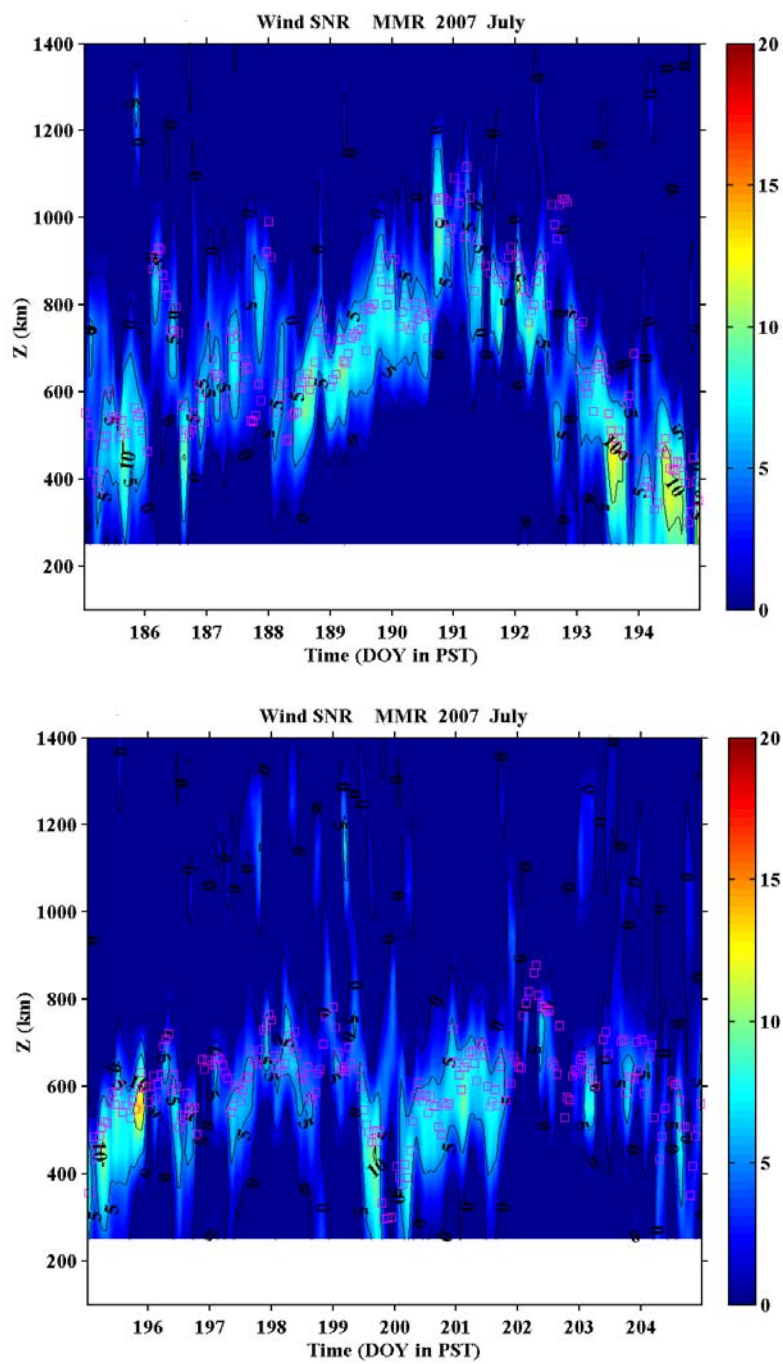
Figure 13.   BLH derived from the SNR method overlaid on SNR variations with time
and height during July 2007 at the MMR site.

Figure 14 shows the effect of quality control of the detected BLH. Here, the 'good' BLH were detected mostly from the low mode profiling. It also shows that nearly all the outliers are biased toward higher BLH. The amount of erroneous BLH suggests that it is necessary to implement the error flag to identify the outliers, which may be associated with clouds or local inversion/moisture decrease at higher levels. In Figure 15, the SNR detected is overlaid on the contour plot of virtual potential temperature. Here, the temperature profiles clearly shows the diurnal variation with daytime warming and nocturnal cooling. However, the SNR detected BLH does not seem to show the similar diurnal variation as illustrated by Stull (1988, Figure 1). The main reason for this apparent discrepancy lies in the detection of BLH at nighttime as the SNR method is not optimal for nighttime BLH detection (to be discussed later in this chapter). Also, we can see that the daytime detected BLH appear to be in the inversion instead of the inversion base. Thus, it is expected that the gradient method may give a lower BLH compared to those from the SNR method.
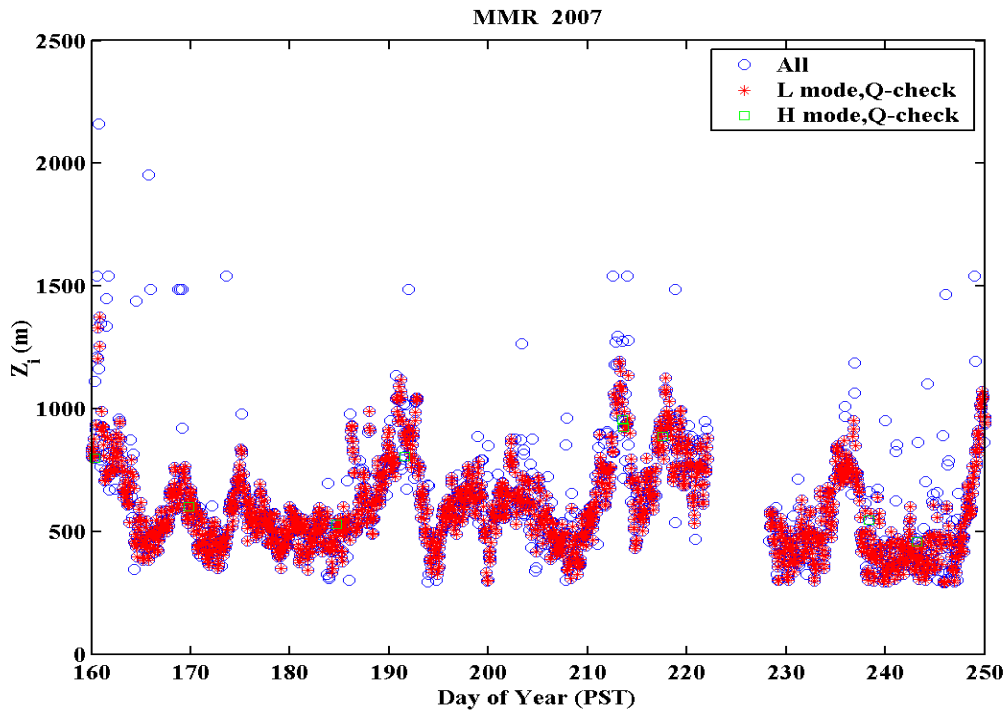
Figure 14.   All BLH detected using the SNR method from both high- and low- mode profiling (blue circle). The red * are the BLH detected from the profiler's low-mode measurements without error flags. The green squares denote the error-free BLH from the high mode measurements. Data were obtained from the MMR site in the summer 2007.
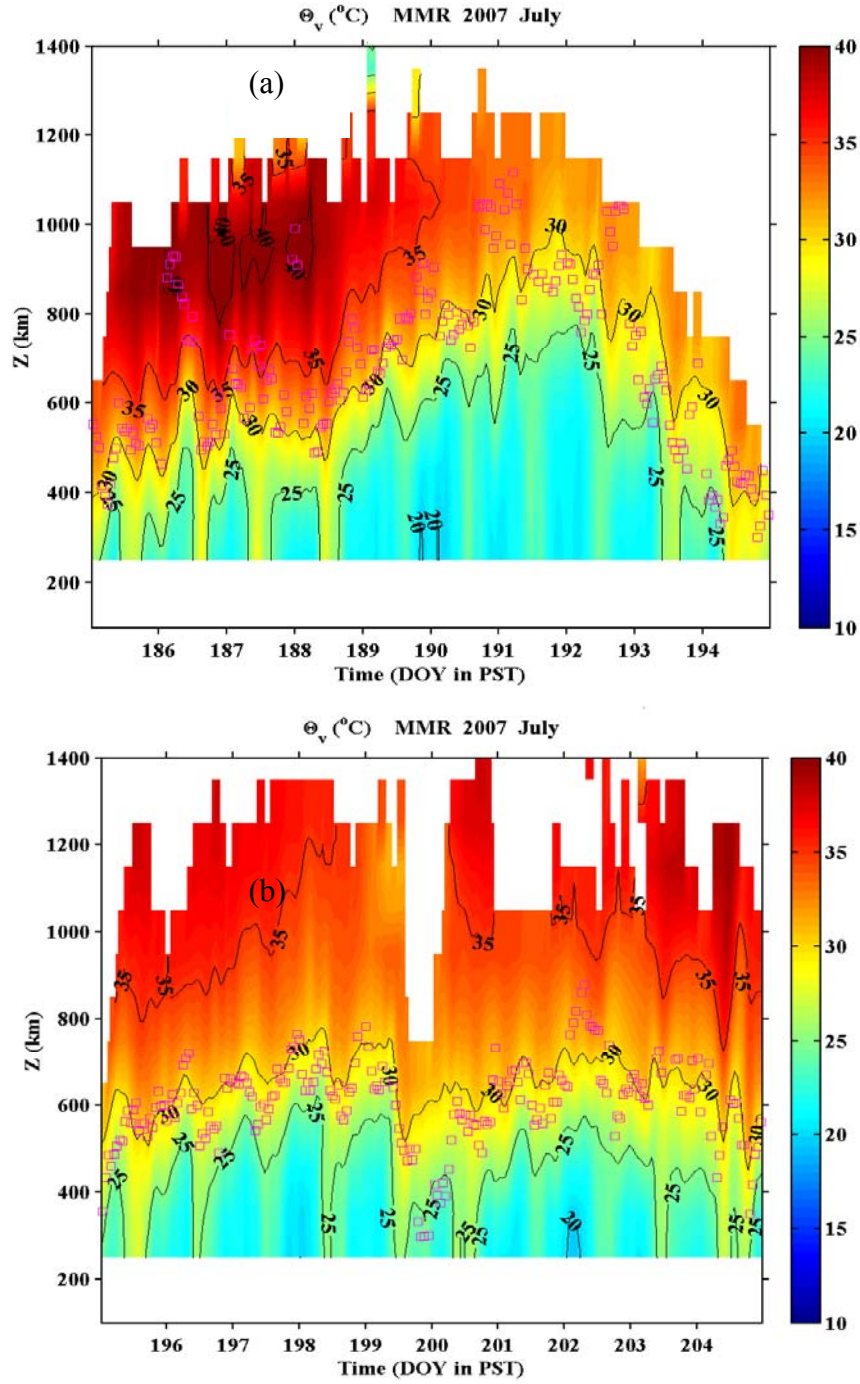
Figure 15.   SNR method detected BLH (pink squares) overlaid on virtual potential temperature for (a) 5-14 Jul 2007 and (b) 15-24 Jul 2007 at the MMR site.

2.   The Gradient Method

The gradient method uses the RASS virtual temperature only without input from the profiler. The idea is to identify the level where the potential temperature gradient exceeds a given threshold. We first derived the virtual potential temperature (θ_v) based on altitude and the measured virtual temperature at each level. The θ_v profile is then over-sampled with linear interpolation at 5 m vertical resolution in order to reduce the low resolution (60 m) effect (binned values) of RASS profile on BLH detection. Then a vertical smoothing of the over-sampled θ_v profile is made using a moving-average with a window equal to the original profile resolution in order to remove the high frequency content introduced by the linear interpolation. The vertical gradient of the θ_v is then calculated based on the smoothed θ_v profile.

Detection of the BLH is made based on comparison of the calculated θ_v gradient with a given threshold of the θ_v gradient. The BLH is defined using a weighted average of the altitudes where θ_v gradient satisfies the gradient requirements, where the weighting is the θ_v gradient at each level. A quality control of BLH values is also applied using the same method as in the SNR profile peak method for the identification of outliers.

Needless to say, the choice the gradient threshold should affect the detected zi. We tested on several values of the threshold compared to visual inspection of the vertical profiles of θ_v. A value of 2°C/100m appear to yield zi values that best matches those subjectively identified from the observed θ_v profiles. In addition, if a profile has less than four levels, which implies low RASS signal, the profile is rejected without going through the gradient detection.

Figure 16 illustrates the BLH detected using the gradient method overlaid on virtual potential temperature profiles. It is seen, indeed, that the gradient detected BLH corresponds to the level with the largest θ_v gradient. The gradient scheme seems to perform as expected.

Figure 16.   Examples of BLH derived from the gradient method (blue dots) overlaid on contours of virtual potential temperature (^{o}C). Data was taken at the MMR profiler site during July 2007.

3.   Evaluation of the NPS Boundary Layer Detection Schemes

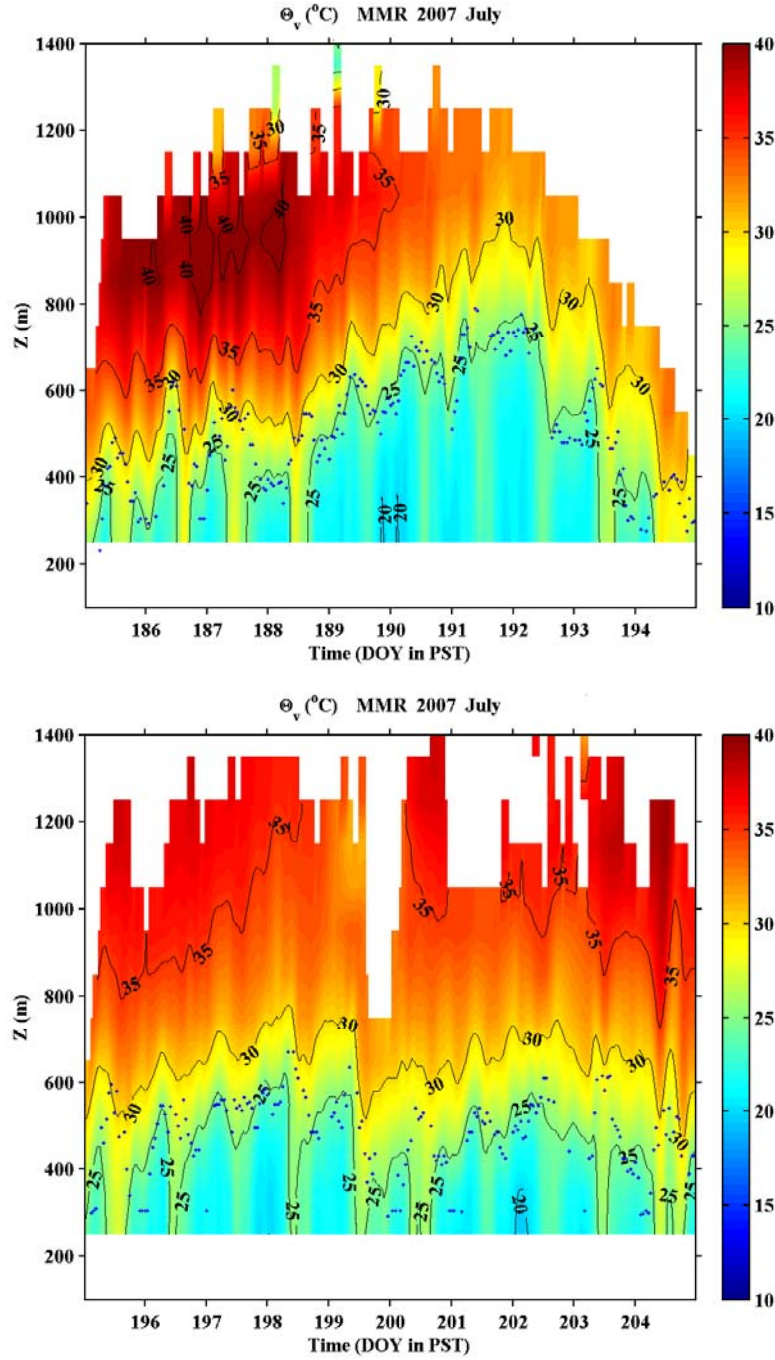Although the NPS half-hourly profiler/RASS measurements were used to develop and test the BLH detection schemes, systematic evaluation of the schemes requires a large amount of data, mainly rawinsonde and profiler/RASS measurements.   The Miramar-San Diego profiler site is chosen for several reasons.   First, it has the twice-daily rawinsonde measurements as well as the hourly profiler/RASS measurements.   Second, its location is within the WRF model simulation domain.   We therefore can use this site for model evaluation.   Thirdly, the inland location of the MMR site is ideal for the occurrence of the clear convective boundary layers, especially during the summer months.   It is thus likely that one can identify sufficient cases of the clear convective boundary layer from this site.   The results on validation of the BLH using both the SNR method and the gradient method will be shown using the MMR site data only.   For this purpose, we obtained BLHs from the twice-daily rawinsonde measurements from July, August, and September in 2006 and 2007.   Boundary layer height from the profiler/RASS system at the same time are also calculated using our BLH detection schemes.   Figure 17 below details the comparison between BLH detected from the SNR and gradient methods for several 10-day periods in the summer of 2007 from the MMR site.   It shows that all three BLHs follow the same general pattern of the boundary layer evolution with, however, some apparent differences.   In general, SNR method yields higher BLH than the gradient method, while the BLH from rawinsonde generally lies in between those detected from profiler/RASS system.   Sometimes, the SNR method tends to overestimate the BLH (e.g. between DOY 213 to 215).   These may be the cases where significant moisture gradients exists above the boundary layer top so that the maximum SNR does not correspond to maximum temperature inversion (results from rawinsonde and gradient method).   On the other hand, the BLH from the gradient method seem to have problem at low levels where its detected boundary layer two persistent values around 200 and 300 m.   This was likely related to the resolution effects when the smoothing schemes does not work well for small amount of input data.   The amount of underestimated BLH near 200

m or 300 m was reduced after the profiles with less than four vertical levels were excluded. There, however, still exists some underestimated BLH for some night time boundary layers.

In general, there is good agreement in the variation of the BLH as they all follow the same general variation. The gradient method appears to detect the lower limit, while the SNR method gives the higher limit of the BLH. More scattering is seen in the SNR method detected heights, particularly when the BL is deep.
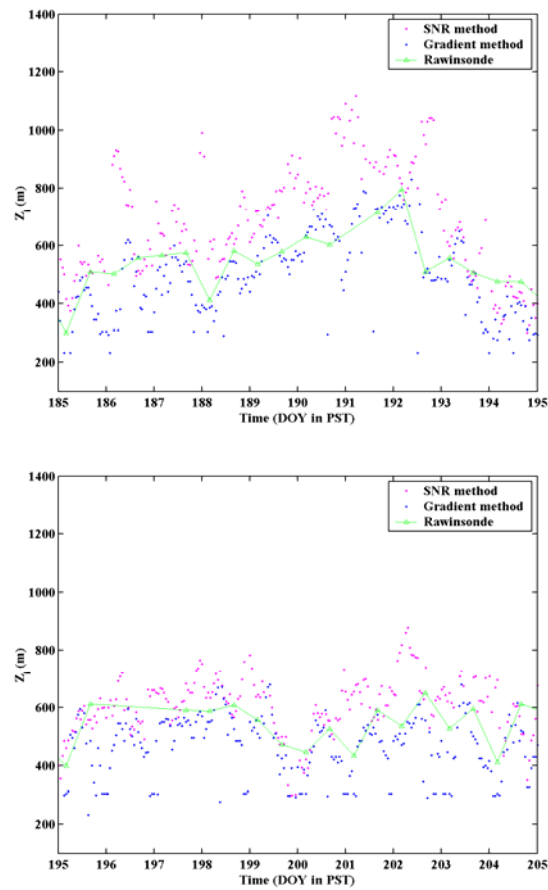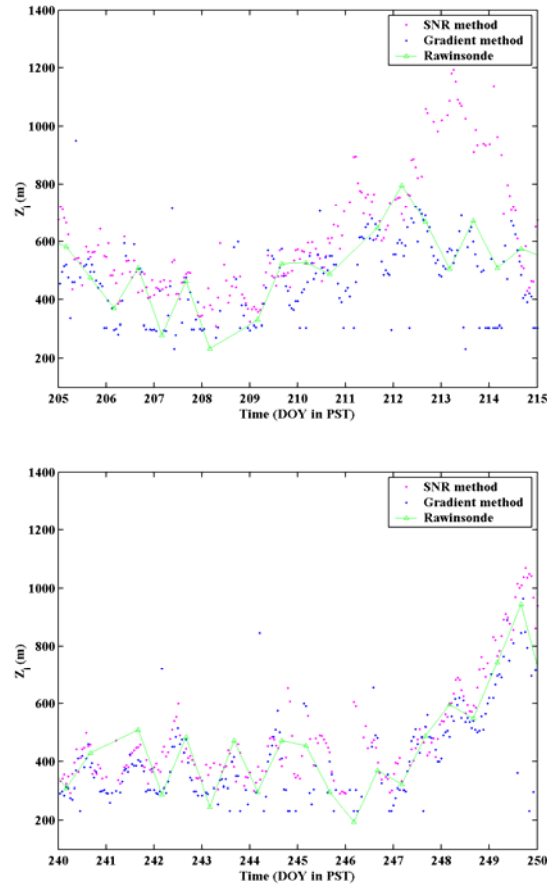
Figure 17.   Comparison of BLH derived from the SNR method, the gradient method, and from rawinsonde profiles during summer of 2007 at the MMR site.

Figure 18 further shows the zi detected from different methods relative to the vertical variation of potential temperature. Again, here the gradient method detects the lower limits of the virtual potential temperature inversion and the SNR method detects the upper limit of the virtual potential temperature inversion. The RASS observed potential temperature shows clearly the diurnal evolution of the boundary layer temperature over land with daytime warming and nighttime cooling. Correspondingly, we also observed the diurnal variation of the boundary layer height that is deeper during the day and shallower at night. This diurnal variation is vaguely seen in the gradient detected zi and some rawinsonde data, but not in the SNR detected zi.

40
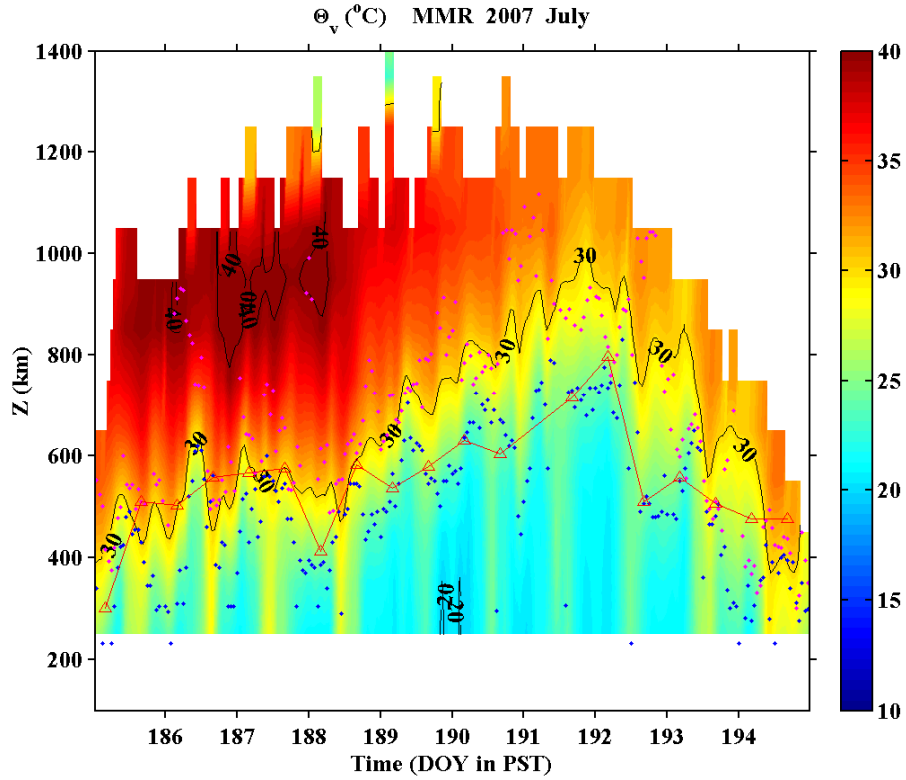
Figure 18.   BLH from all three methods overlaid on a cross section of virtual potential temperature during July 2007 at the MMR site. The blue dots represent the BLH from the gradient method and the pink dots represent the BLH from the SNR method. Rawinsonde BLH are the connected red triangles.

Table 2 below summarizes the comparison between rawinsonde detection and the SNR and gradient methods of BLH detection. All data from the summer month of 2006 and 2007 at MMR site are included in this table. In general, the SNR method gives higher BLH but may overestimate the BLH, particularly at night. Rawinsonde results show lower BLH at night which is also seen in the gradient method, but not in the SNR method. Apparently, the SNR method is problematic at night as its nighttime detected BLH is even larger than its daytime values. However, it should be kept in mind that this comparison is not accurate, as the measurements were not necessarily made at the same time. Further comparisons will be made in tables and figures shown later when the z_i pairs from the same time are compared. The amount of data available for the SNR and

41

gradient detection method are the same, however, the gradient method shows more detected BLH than the SNR method, suggesting that the gradient method did not reject as many measurements as the SNR method. Hence, the total number of BLH detections from the gradient method is not limited by the limited number of height levels in the return signal of RASS at this site. This may change if the boundary layer is deeper at a different site.

When compared with rawinsonde, BLH from the SNR method is more variable. The gradient method, on the other hand, is less variable as seen from the standard variation of the detected BLH.

Table 2.   Comparison of BLH derived from rawinsonde, SNR method, and gradient method at the MMR site during summer months of 2006 and 2007.

		Rawinsonde	SNR	Gradient
Number of data	Day	152	746	811
	Night	154	1699	1993
	total	306	2445	2804
Mean Zi height	Day	569	639	533
(all data)	Night	518	651	464
	Total	543	647	484
Zi standard deviation	Day	147	264	103
	Night	232	297	149
	total	196	288	141
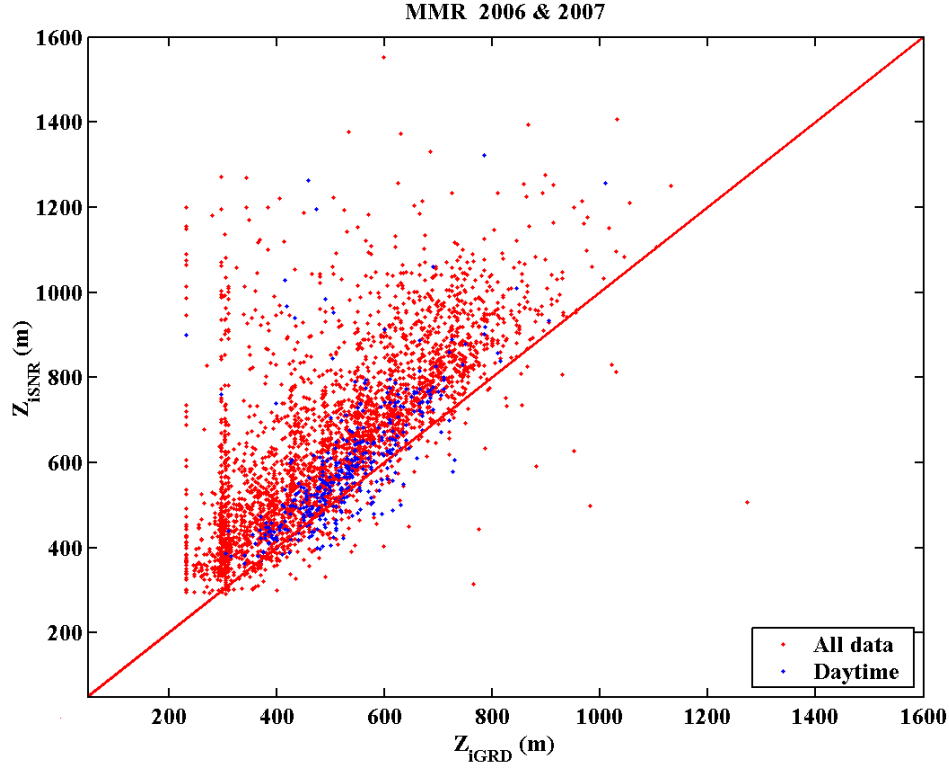
Figure 19.   Comparisons between the SNR and gradient methods of BLH detection. Data is taken from the MMR profiler site during the summer months of 2006 and 2007.

Figure 19 shows a direct comparison of the z_i from the SNR method and the gradient method. The diagonal red line represents perfect correlation. The data used is the same as those in Table 2, except that only z_i obtained from the two methods are within 10 minutes of time difference are used for fair comparison. The total amount of data points is thus less in Figure 19 compared to those shown in Table 2. A summary of the comparison of the same data points is given in Table 3 along with the comparison with z_i from the rawinsonde data. From Figure 19, the tendency of the SNR method to detect higher z_i than the gradient method is clearly seen for all data as well as for the daytime BLH. However, the difference for the daytime z_i is 64 m (Table 3), which is very close to the vertical resolution of the profiler and RASS.   The mean correlation of the z_i from the two methods is close to 70%. Also, the problem of the gradient method in false detection of low z_i at around 200 and 300 m is also clearly seen in Figure 19.

43

Validations of the zi from the two methods are made through a thorough comparison with the rawinsonde zi made within 10 minute of each other shown in Figures 20 and 21. Since the rawinsonde measurements were made only twice daily, the data points for this comparison is limited, but is large enough to indicate the validity of out detection methods. The SNR method gives very good mean BLH during the daytime with a difference of less than 5 m (Table 3 and Figure 20). The nighttime mean BLH is overestimated by 96 m (Table 3). Hence, our results are suitable for the daytime CBL and further study will need to be done on nocturnal BL to determine the most accurate method of detection.
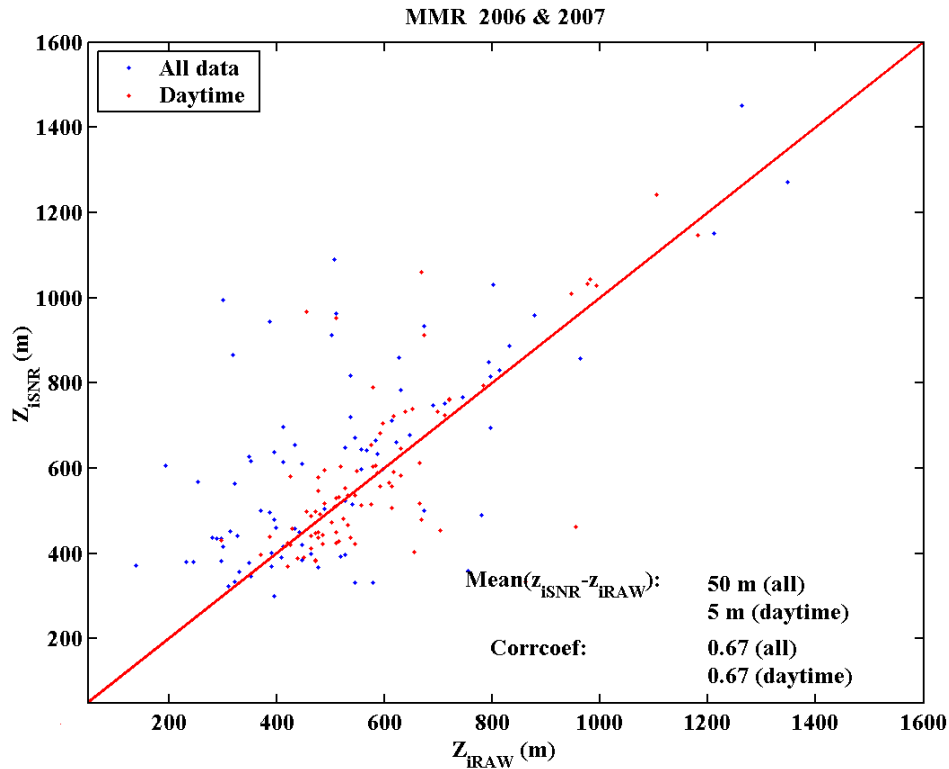
Figure 20.   Correlation between SNR derived BLH and rawinsonde BLH for the MMR site during summer months of 2006 an 2007.

The gradient method give a mean underestimates of about 47 m for the daytime and 59 m at night. The bias is larger compared to the SNR method, however it is still within the magnitude of the vertical resolution of the wind profiler. The gradient method

44

detected BLH is, however, better correlated with the rawinsonde zi, particularly at night (86%). The correlation during the day is at 72%, slightly better than the SNR method. Thus the gradient method does a better job for the nighttime detection of the BLH with smaller mean discrepancy and less scatter.
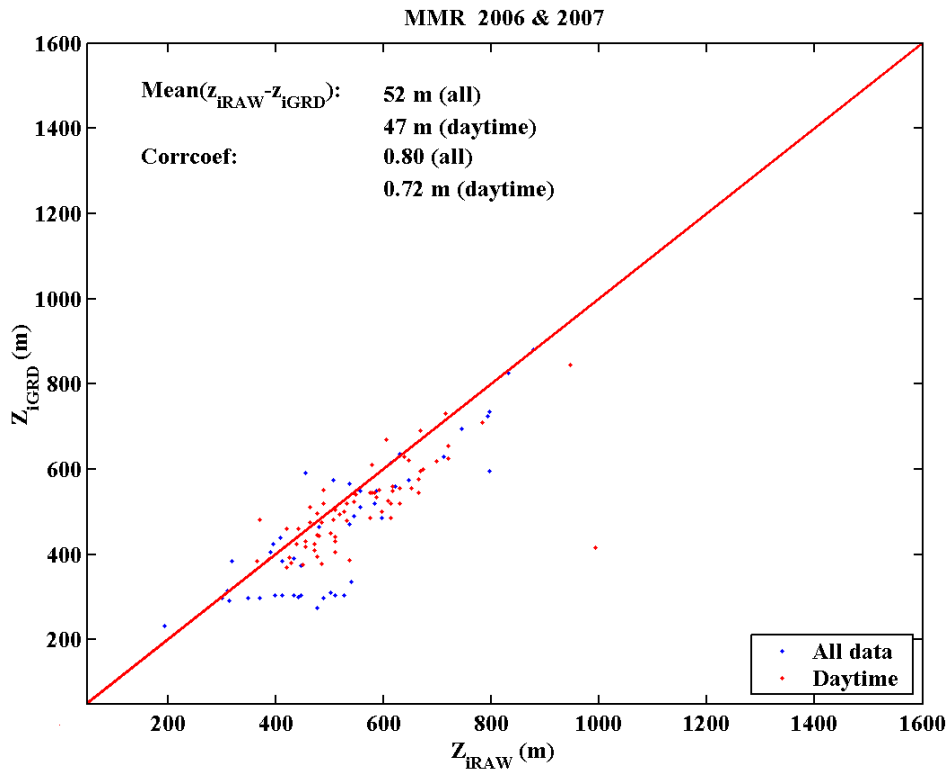
Figure 21.   Correlation between gradient method derived BLH and rawinsonde BLH for the MMR site during summer months of 2006 and 2007.

Table 3.   Comparison of BLH from SNR and gradient methods against rawinsonde BLH at the same time. All data are from the MMR site during summer months of 2006 and 2007.

		Rawinsonde	SNR	Diff (Raw-SNR)	Rawinsonde	Gradient	Diff(Raw-GRD)
Number of data	Day	85	85		115	115	
	Night	85	85		115	115	
	Total	170	170		230	230	
Mean Zi height	Day	585	590	-5	559	511	47
	Night	521	617	-96	518	459	59
	Total	553	603	-50	542	491	52
Zi standard deviation	Day	164	199	143	118	95	82
	Night	227	239	186	153	162	83
	Total	200	220	172	134	128	82
Corrcoef	Day			0.6723			0.7202
	Night			0.6683			0.8634
	Total			0.6692			0.8037

The box-and-whisker plot below (Figure 22) shows the major characteristics of the distribution of the deviations of the SNR z_i and gradient z_i from rawinsonde z_i. The left set of box plots shows larger spread of the results for both day and night than the plots on the right with more outliers. The nighttime boxplots also reveals the significant skewness toward larger detected z_i from the SNR method and the apparent negative skewness towards smaller z_i from the gradient method. The variation for the daytime is much smaller and not obviously skewed.   These same features are clearly seen in the histograms shown in Figure 23.
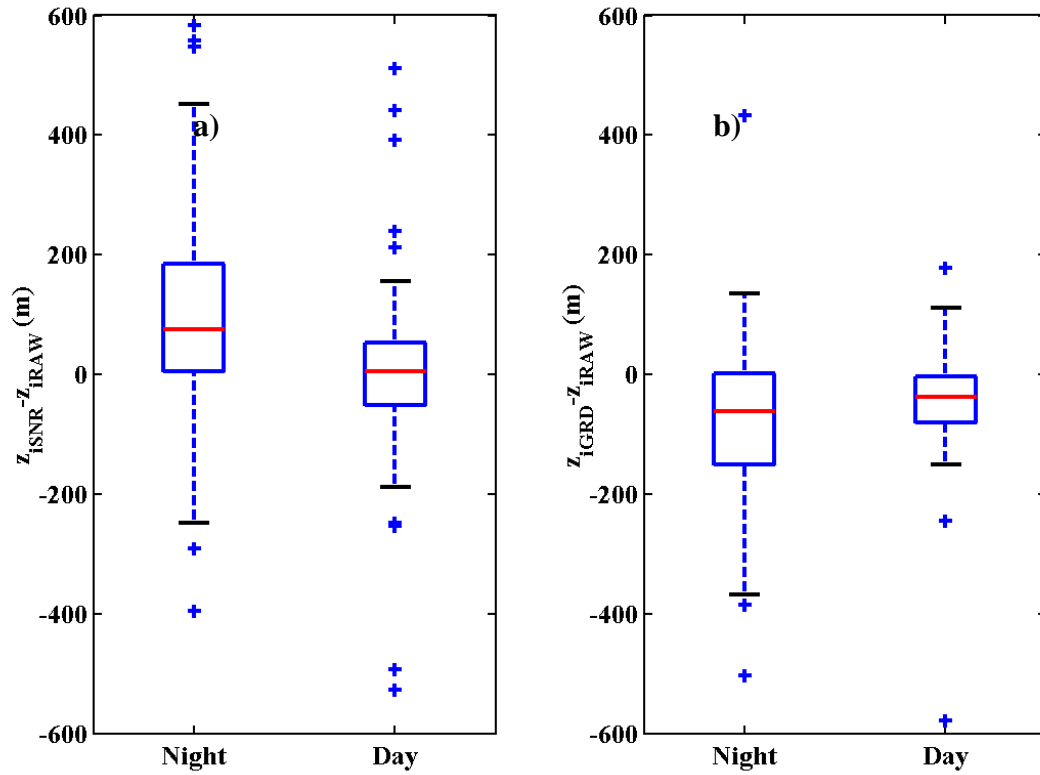
Figure 22.   Box and whisker plots comparing the major statistical characteristics of a) the deviation of SNR detected zi from those from rawinsonde and b) the deviation of the gradient method detected zi from those from rawinsonde at the MMR site during the summer months of 2006 and 2007. The red lines denote the median. The boundaries of the box denote the upper and lower quartile. The whisker length is 1.5×IQR.
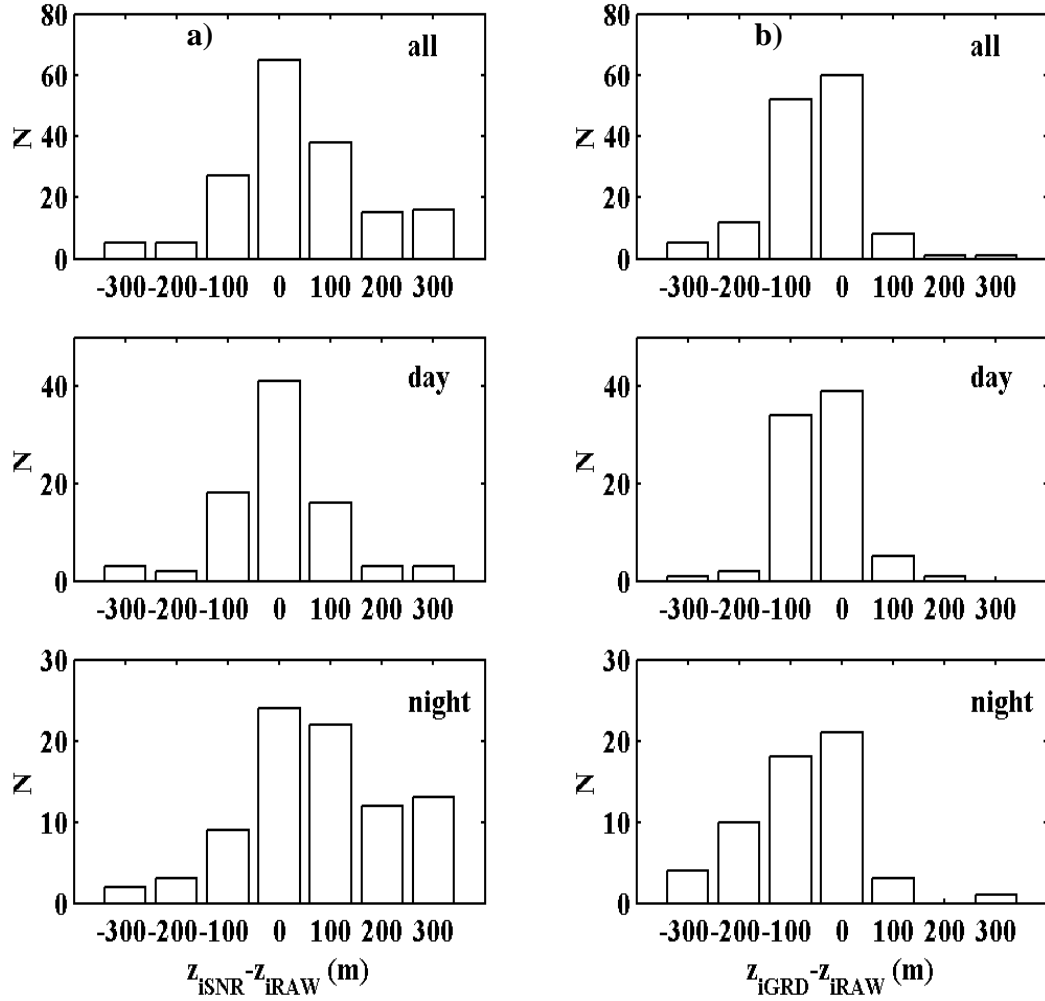
Figure 23.   Histograms comparing statistics of a) difference between the zi from the SNR method and those from rawinsonde and b) difference between the zi from the gradient method and those from rawinsonde at the MMR site during the summer months of 2006 and 2007.

V. WRF MODEL SIMULATIONS AND RESULTS

A. WRF-ARW (ADVANCED RESEARCH WRF) MODEL SIMULATIONS

The WRF simulations were made by The Aerospace Corporation. WRF-ARW (Advanced Research WRF) model version 2.2 is used in this study. It is configured to use the ETA-TKE follow on PBL scheme, and the NOAH Land Surface Model (LSM), which has four soil layers. The 15 km outer domain and 5 km inner domain were initialized using the 30-second (0.9 kilometer) terrain data. The outer and inner domains interact. The model atmosphere uses 37 vertical levels with the top pressure of 100 hPa. The Rapid Radiative Transfer Model (RRTM) radiative transfer scheme within the model is used with a 30-minute radiance time step (Mlawer et al., 1997), along with the cumulus parameterization of Grell (Grell et al., 1994). Initial and lateral boundary conditions are provided by the NCEP North American Model (NAM) at 40 km grid spacing. Figure 24 below shows the model inner domain and the corresponding terrain height for this study. The domain covers a portion of southern California which includes the MMR site. In addition to the MMR site, locations of four other profiler sites are also shown on this figure. Results from these sites will be studied in future efforts.
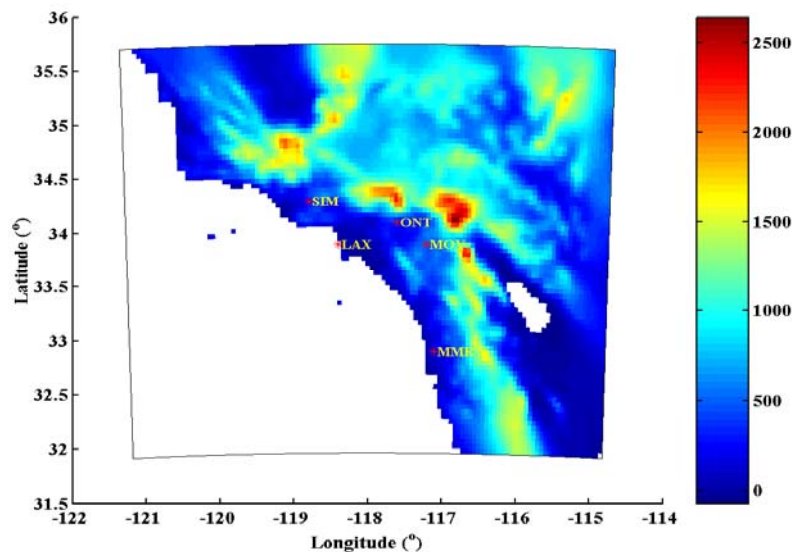
Figure 24. WRF-ARW inner domain terrain heights (m). It covers southern California and includes the MMR site as well as four other sites.

The Aerospace Corporation WRF simulations were made continuously for the period of July, August, and September of 2007. The daily WRF simulations over southern California produces hourly forecasts out to 72 hours. For our study, we used the 13-36 hr forecast from each daily run to form a time series of the entire three month except for a few days when forecasts were not available. The original WRF outputs are in NETCDF data format. A MATLAB code was created to read the NETCDF data file for specific variables and time periods needed for this research. The resultant WRF data were then stored in MATLAB format.

B.   WRF GENERAL RESULTS

Figure 25 shows the time series of several basic thermodynamic and surface variables from 10 days of WRF simulation. The diurnal variation is seen distinctly in the surface and air temperature, as well as in U component of the mean wind. The Aerospace WRF simulations appear to depict the sea breeze circulation and diurnal cycle rather well. The comparison of the surface and air temperature (Figure 25b) also shows the occurrence of daytime surface driven convective boundary layer and nocturnal stable boundary layer.
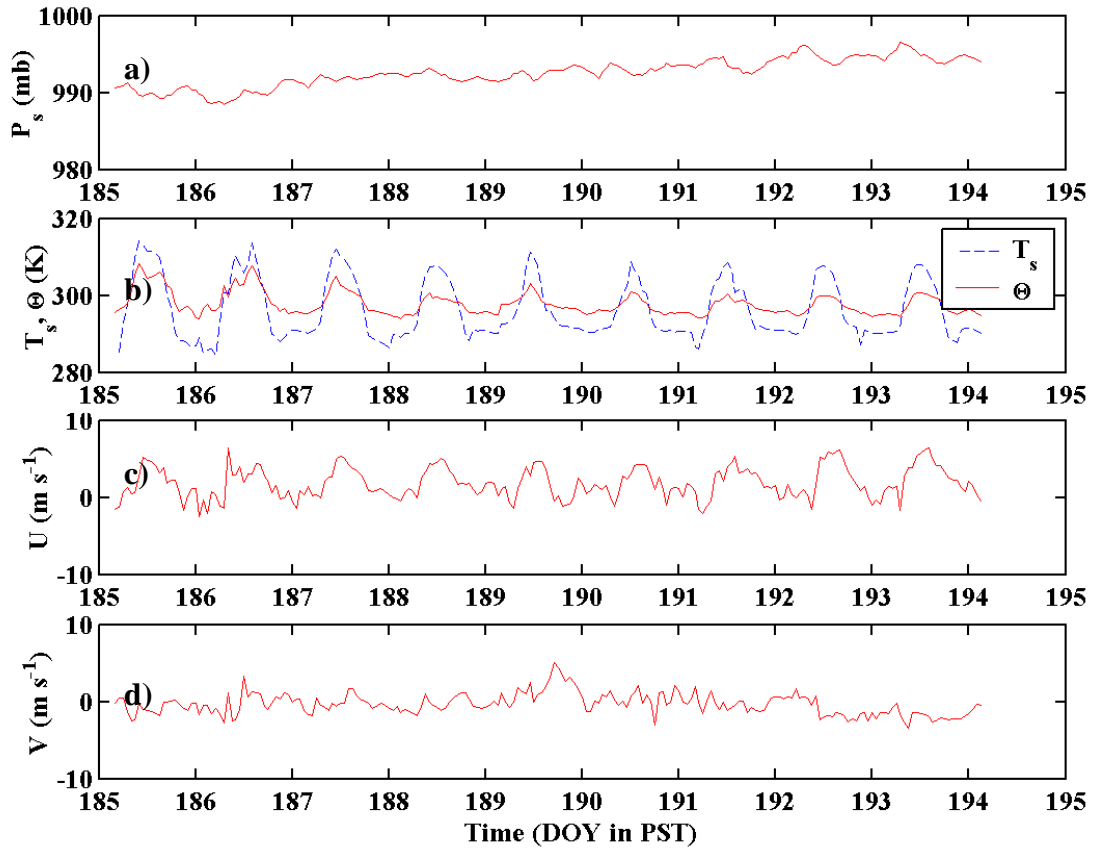
Figure 25.   Results from WRF simulations; a) pressure, b) surface temperature and potential temperature, c) u component of the mean wind, d) v component of the mean wind. Data is taken from a 10-day period in July 2007 at the MMR site.

Figure 26 below shows the WRF predicted virtual potential temperature profiles in comparison with RASS observations. The two panels in Figure 26 are very similar, suggesting that the WRF simulated temperature field can represent the gradual increase of the boundary layer well. Figure 26 also depicts well the diurnal variation of the boundary layer with the expected daytime warming and nighttime cooling. However, the nighttime temperature appears to be lower than that measured by RASS. From the potential temperature profiles, one can see that the WRF predicted boundary layer, subjectively identified from the θv profile, is lower than what the RASS measurements show.

51
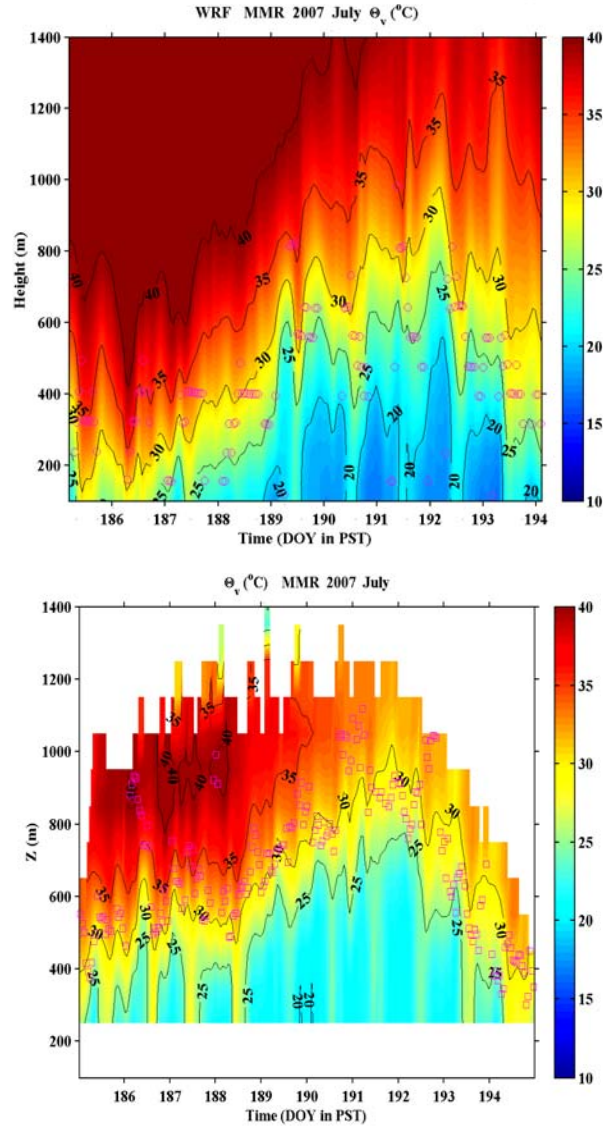
Figure 26.   Time-height cross-section of potential temperature from (a) WRF forecast and (b) RASS measurements at MMR site. The pink circles on (a) denote the WRF diagnosed BLH. The pink square on (b) is the BLH detected from the profiler SNR profiles.

The WRF diagnosed BLH on Figure 26a show slight trend of growth as the BLH grow deeper from day 188 to day 192. However, the diagnosed BLH are mostly within the model forecast inversion layer. This is different from the SNR detected BLH (Figure 26b), which follows the development of the BLH rather closely, although these BLH are

also within the RASS measured inversion. The water vapor specific humidity (Figure 27) shows the forecast boundary layer more clearly due to the presence on a sharp q_v gradient at the top of the boundary layer. From Figure 27, one can identify two groups of the diagnosed boundary layer height: the daytime BLH that are above the forecast boundary layers and the night BLH that are at a constant level (77 m). The latter is not seen in Figure 26 because of the lower limit of the vertical axis is set at 100 m for easy comparison with the RASS observations. From Figures 26 and 27, we can conclude that the bulk Richardson number based diagnoses of BLH is not consistent with the forecast boundary layer thermodynamics.
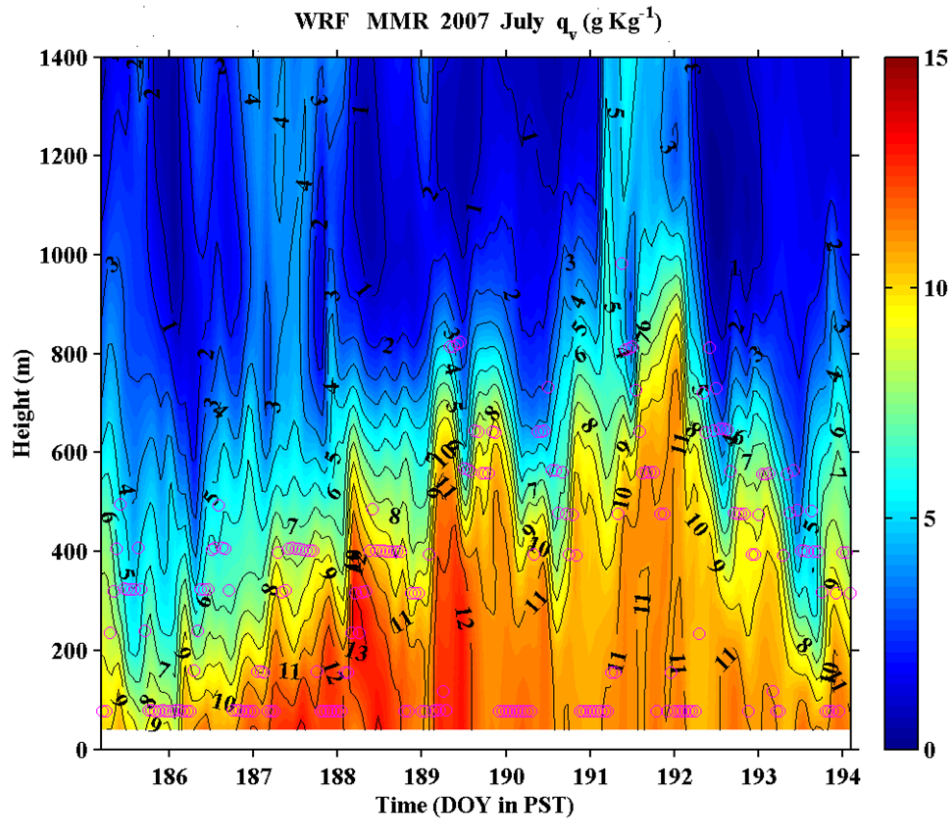
Figure 27.   Same as in Figure 26a, except for specific humidity.

Figure 28 shows an overall comparison of WRF derived BLH compared to the SNR method, the gradient method, and rawinsonde for the MMR site during the entire summer of 2007. Upon initial inspection of the figure, we can see that the WRF BLH is

limited by the model vertical resolution within the boundary layer. And the WRF BLH does not seem to be consistent with any observed BLHs. A zoomed-in look at a 10-day period (Figure 29) during this same timeframe shows that WRF seems to follow the general pattern of boundary layer growth. but again it is overestimated on some days and underestimated on others. The very low BLH detected at the bottom of the image are mainly from the nighttime.
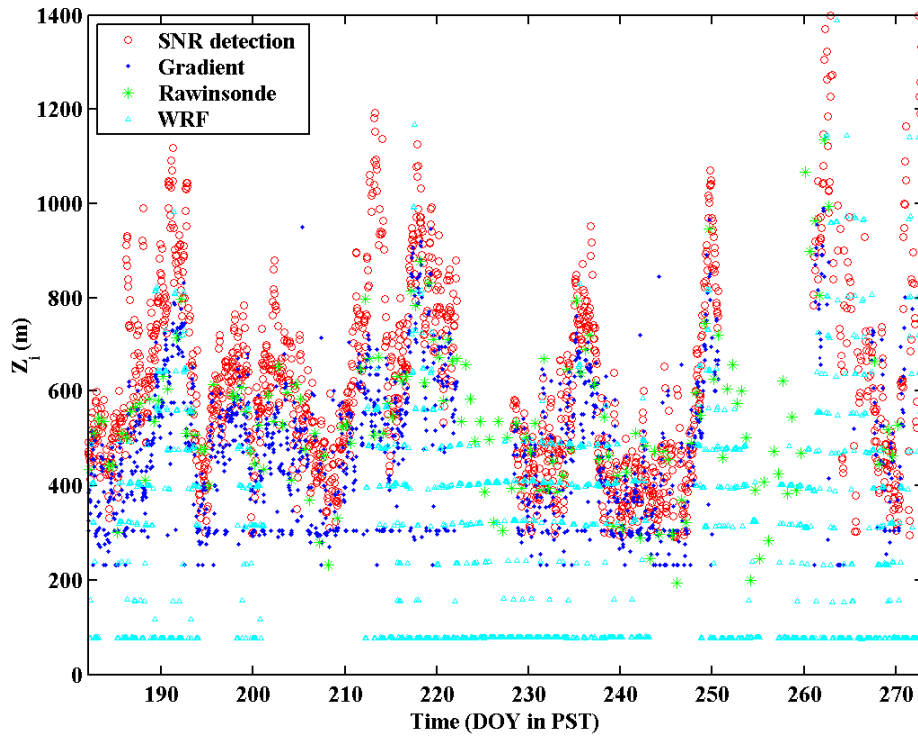
Figure 28.   Boundary layer height from the WRF model, SNR method, gradient method, and rawinsonde for the entire summer of 2007 at the MMR site.
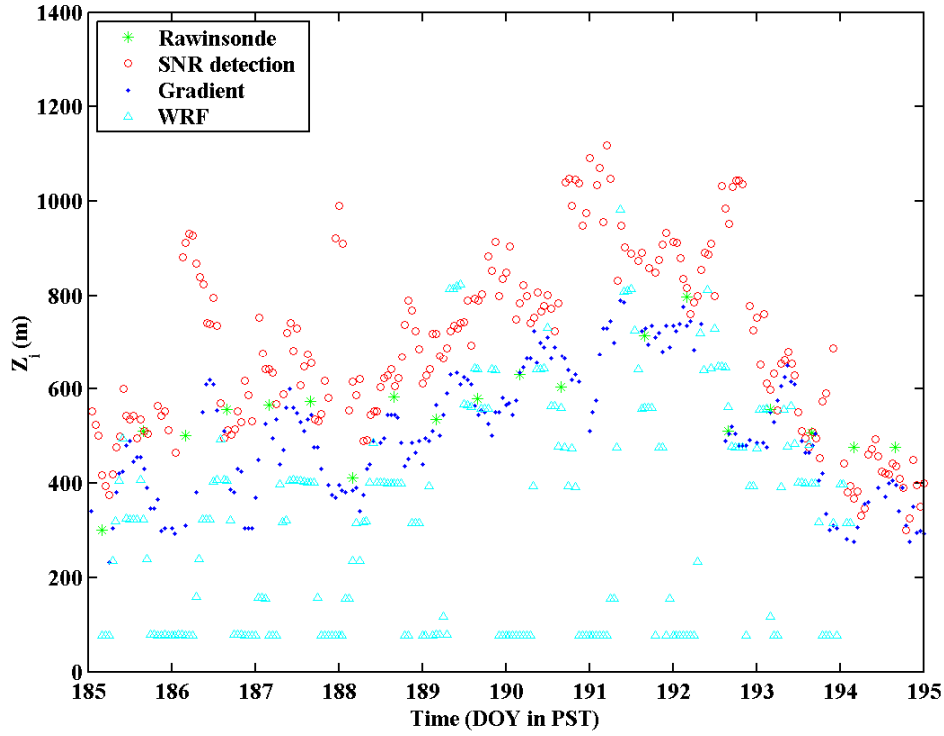
Figure 29.　Same as Figure 28, except for a 10-day period in July only.

Figures 30 and 31 shows the comparison between the WRF derived BLH and BLH from the SNR method and with the BLH from the gradient method for the entire summer in scatter plots. WRF tends to underestimate the BLH as seen in both figures. In the daytime convective boundary layer case, the mean WRF BLH is about 151 m lower than the SNR detected BLH and 95 m lower than the gradient detected BLH. In chapter IV, we identified that the true BLH is in between the SNR and gradient detected BLHs. Thus, the current BLH from WRF is between 95 and 151 m lower than the actual BLH. It is alarming that the overall correlation between the WRF BLH with the observed BLH (SNR or GRD) is small at about 50%. In fact, the Richardson number based BLH is not correlated with the WRF predicted thermodynamic fields, as discussed in Figures 26 and 27. Table 4 summarizes all the relevant statistics related to the inter-comparison.

55
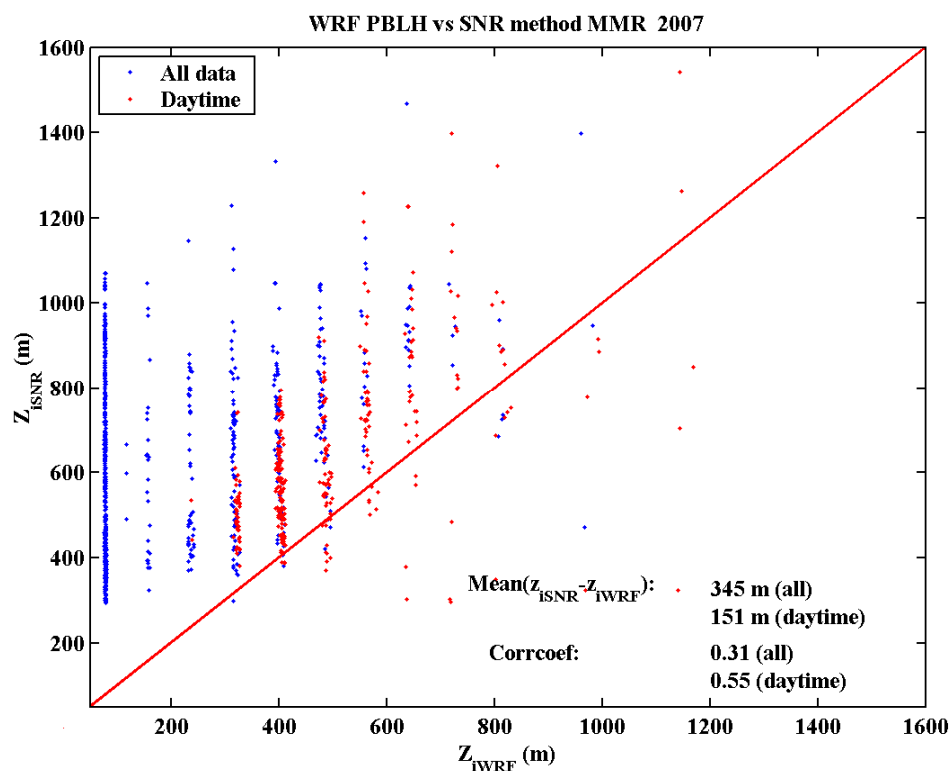
Figure 30.   Comparison between WRF derived BLH and SNR method BLH for the MMR
site during summer 2007.

WRF PBLH vs Gradient Method MMR 2007

Mean(z_{iGRD}-z_{iWRF}): 231 m (all)
95 m (daytime)
Corrcoef: 0.40 (all)
0.51 (daytime)

All data
Daytime

Z_{iGRD} (m)

Z_{iWRF} (m)
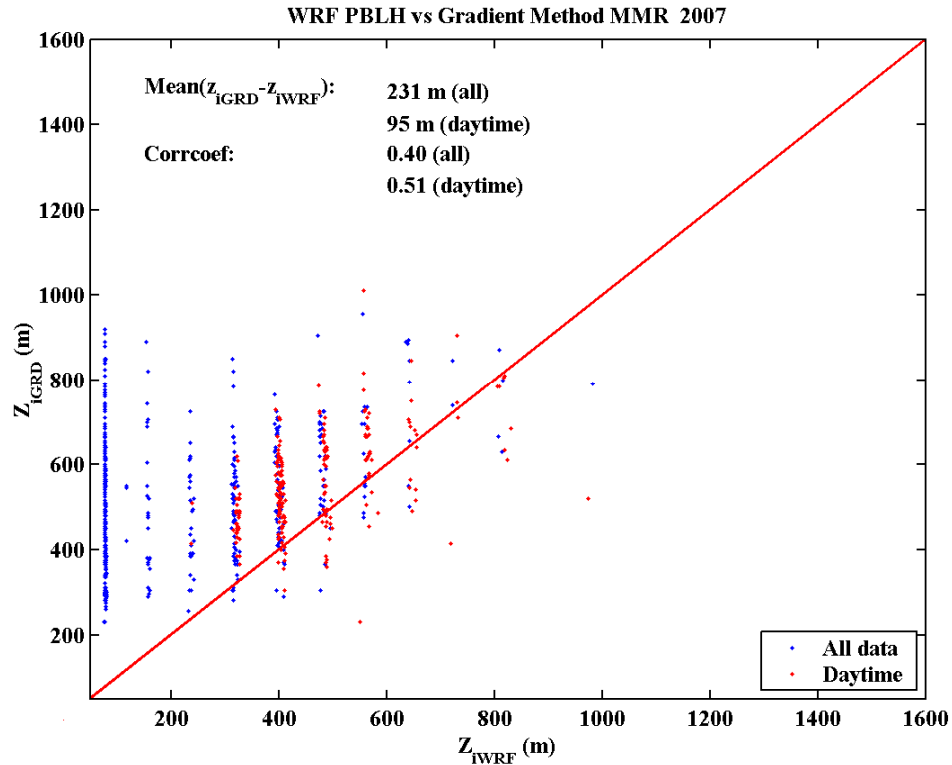
Figure 31.   Comparison between WRF derived BLH and gradient method BLH for the MMR site during summer 2007.

Table 4.   Summary of the relevant statistics from the comparison between the WRF model output of BLH using the Richardson number method and the SNR and gradient methods of BLH detection from profiler/RASS for the MMR site during summer of 2007.

Zi from WRF are obtained from the WRF model output based on bulk Richardson number							
		WRF	SNR	WRF-SNR	WRF	GRD	WRF-GRD
N	All	1054	1054		770	770	
	Day	333	333		231	231	
Mean	All	302	647	-345	287	518	-231
	Day	498	649	-151	465	560	-95
Std	All	219	208	251	199	152	196
	Day	159	195	171	121	113	115
Corrcoef	All			0.3059			0.396
	Day			**0.5509**			**0.514**

57

C. TESTING OF AN ALTERNATIVE METHOD OF BLH DETECTION FROM WRF OUTPUT

Accurate boundary layer height from the mesoscale model is dependent on two equally important factors. First, the model should be able to forecast the boundary layer vertical structure well; and second, the diagnostic boundary layer height detection scheme should identify the BLH that is consistent with the model forecast boundary layer properties. As we have seen from the previous discussions, for the daytime boundary layers, the forecast boundary layer temperature is similar to those observed by RASS with similar time evolution, but the vertical structure is somewhat different with the WRF temperature field showing a lower boundary layer height and lower nighttime temperature. Improvements of the forecast of boundary layer structure relies on many components of the mesoscale model, including its surface flux parameterization and turbulence parameterization and is beyond the scope of the current thesis. Here, we attempt to explore a new BLH detection scheme to replace the Richardson number based scheme. The objective is to obtain BLH that is consistent with the forecast boundary layer structure.

It was seen in Chapter IV that the gradient method results in better correlation with the rawinsonde boundary layer height even though the mean BLH is slightly underestimated. The same gradient method is applied to the WRF forecast potential temperature field using the same gradient threshold of 2 ^{o}C/100m. An example of the result is shown in Figure 32 below, where the pink circles are the Ri number BLH and the yellow dots are the gradient derived BLH. This method produced even lower boundary layer height, but the results are consistent with the modeled boundary layer. This method also appears to improve some underestimates of the nighttime BLH when the actual WRF boundary layer top is at levels much higher than a constant 77 m from the bulk Richardson method (DOY 190-193) . It is seen in Figure 33 that the gradient detected BLH is also consistent with the base of sharp specific humidity gradient.
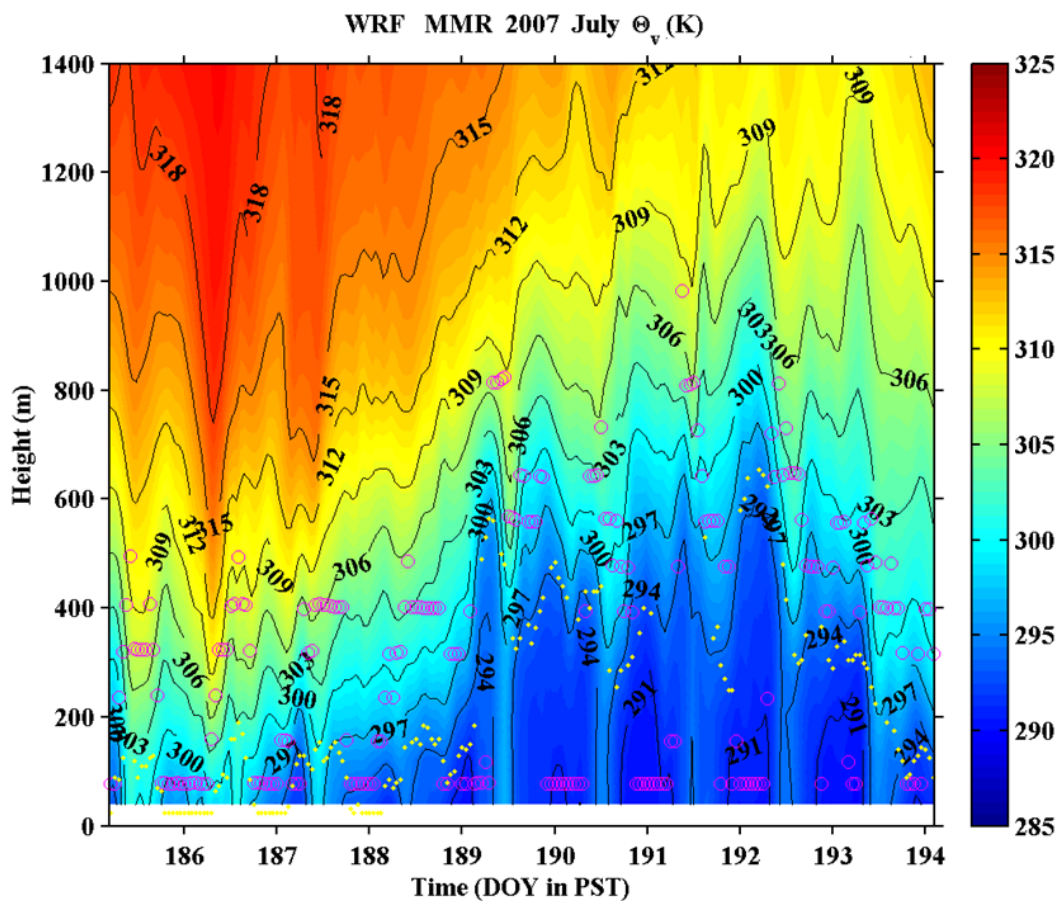
Figure 32.   Comparison of the WRF boundary layer height from the Richardson number method (pink circle)and the boundary layer height diagnosed from the WRF potential temperature field using a gradient method (yellow dots) at the MMR site during July 2007. Data points are overlaid on contours of virtual potential temperature.
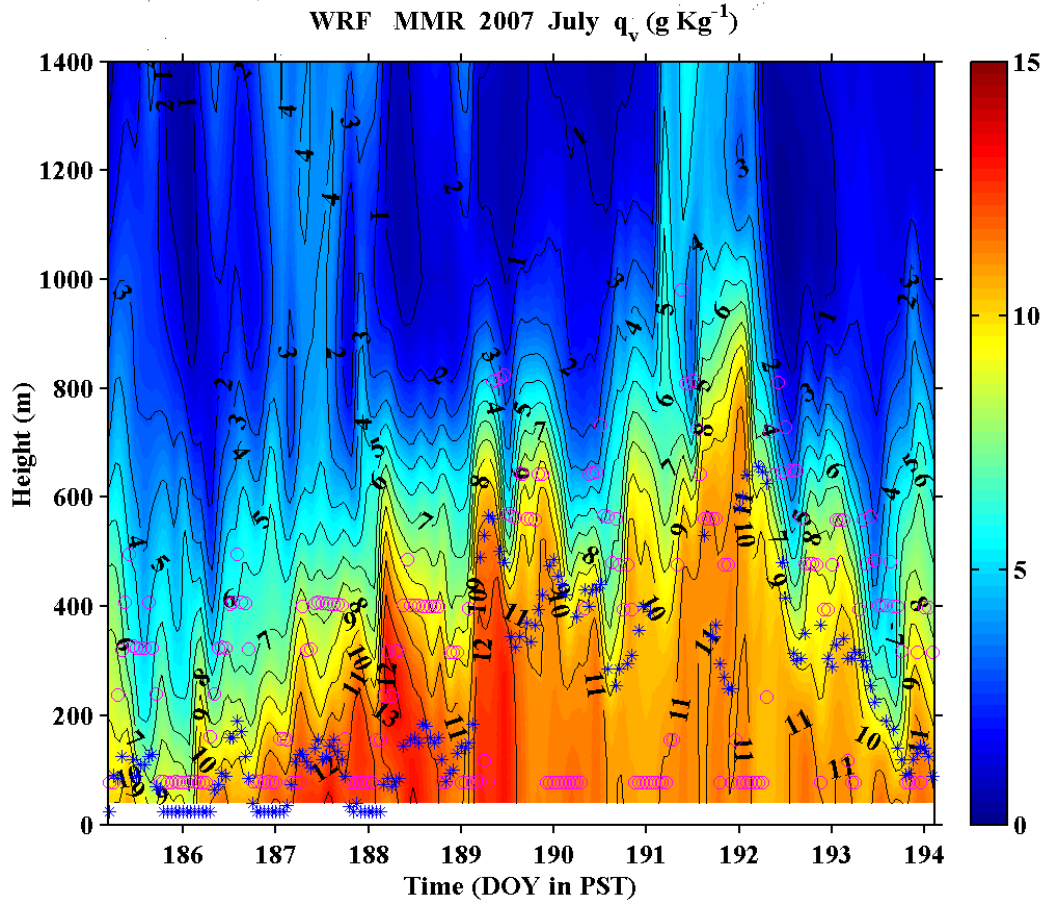
Figure 33. Same as in Figure 32 except for specific humidity and the gradient detected WRF BLH is shown as blue *.

Figure 34 shows a comparison between the SNR method, the gradient method, rawinsonde, WRF Richardson number derived, and WRF gradient method derived BLH's. The gradient method detected WRF BLH is apparently much lower than the observations. However, it better depicts the boundary layer height variations that show consistency with the observed BLH's.
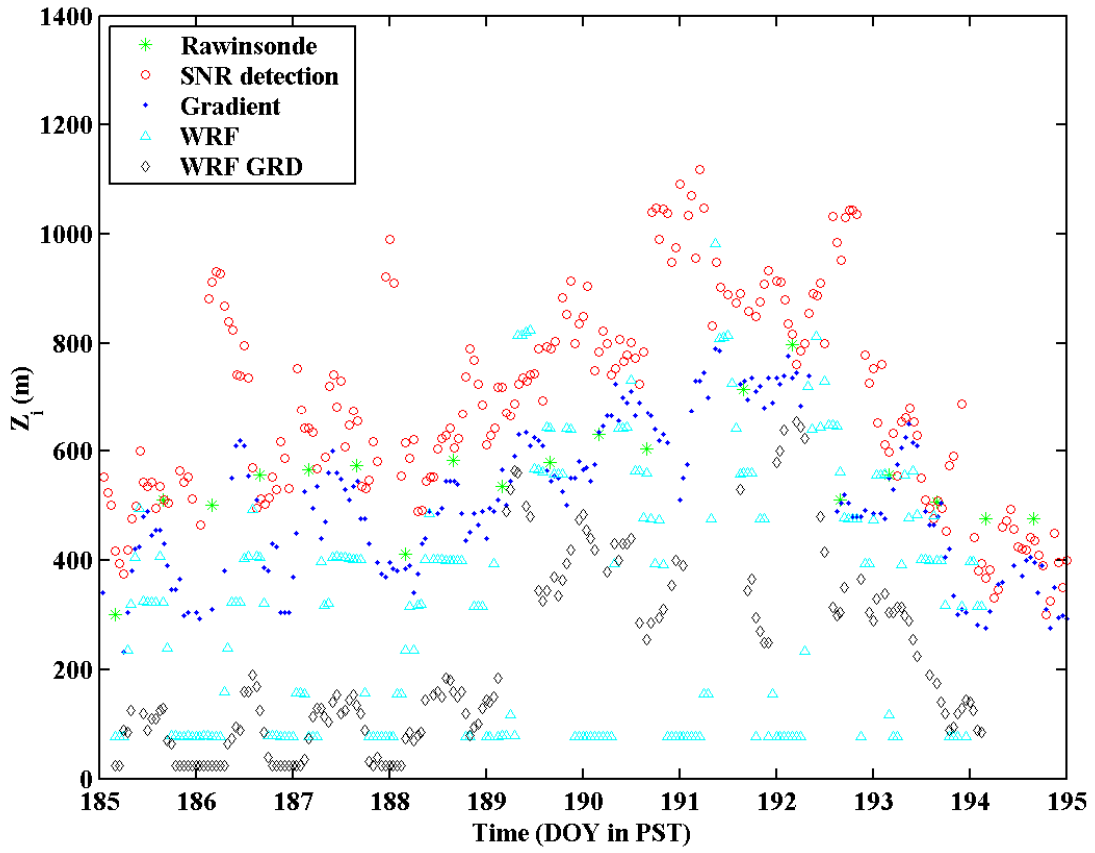
Figure 34.　Comparison of BLH detection from rawinsonde, SNR method, gradient method, WRF Richardson number, and WRF gradient method. Data is taken from the MMR site during July 2007.

The better correlation between the gradient detected WRF BLH and the observations are best seen in the scatter plots of Figures 35 and 36. Although with the much lower BLH, Figures 35 and 36 show improved correlation between the WRF gradient method BLH and RASS (0.70) and the SNR method (0.58). A summary of the comparison can be seen in Table 5. Compared to results in Table 4, Table 5 shows that the gradient method significantly improved the BLH detection at nighttime although comparison with the gradient method BLH from the RASS measurements for the daytime cases also improved slightly.
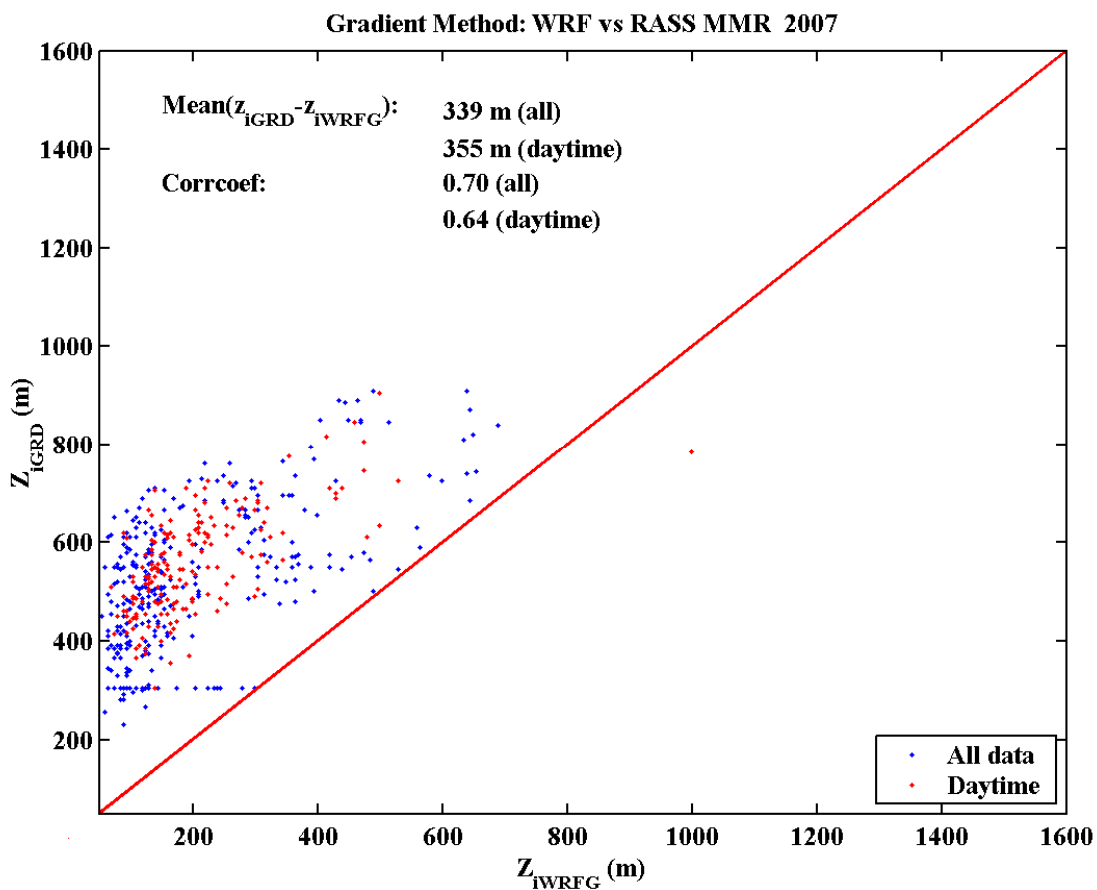
Figure 35.   Correlation between WRF gradient method of BLH detection and gradient method from profiler/RASS for the MMR site during summer 2007.
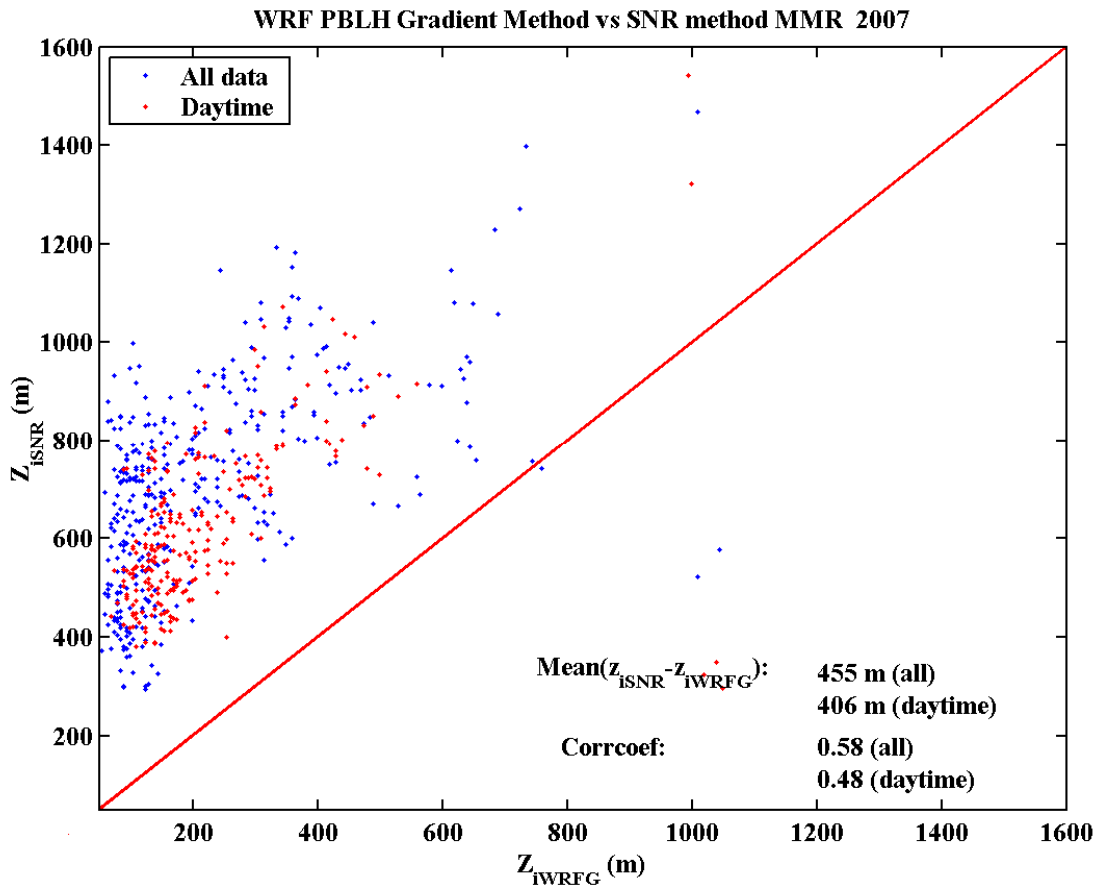
Figure 36.   Correlation between WRF gradient method of BLH detection and SNR method from profiler/RASS for the MMR site during summer 2007.

Table 5.   Summary of the comparison between the WRF model output of BLH using the gradient method and the SNR and gradient methods of BLH detection from profiler/RASS for the MMR site during summer of 2007.

Zi from WRF are obtained from the WRF model output using gradient method							
		WRF	SNR	WRF-SNR	WRF	GRD	WRF-GRD
N	All	796	796		601	601	
	Day	243	243		183	183	
Mean	All	173	629	-455	168	506	-339
	Day	220	626	-406	203	558	-355
Std	All	164	202	171	137	144	108
	Day	153	166	162	113	104	92
Corrcoef	All			0.5811			0.7014
	Day			**0.4849**			**0.6446**

THIS PAGE INTENTIONALLY LEFT BLANK

VI. CONCLUSIONS AND RECOMMENDATIONS

A. SUMMARY AND CONCLUSIONS

This thesis study focuses on the evaluation of the boundary layer height (BLH) diagnosed from a mesoscale model in comparison to wind profiler/Radio Acoustic Sounding System (RASS) measurements from the wind profiler site at Miramar Marine Corps Station (MMR). This objective is met through validation of the observed BLH and evaluations of the model BLH using the observed BLHs.

The data used for this research was mainly collected at the Miramar-San Diego profiler site where measurements of a 915 MHz wind profiler with RASS system are available hourly. Twice daily routine rawinsonde measurements are also available. In addition, the site is within the WRF model inner domain so that we can use the measurements to evaluate WRF diagnosed boundary layer height. For validation of our boundary layer height detection scheme, we used data from July, August, and September in 2006 and 2007. For model evaluation, data from summer of 2007 were used.

We have developed two methods to detect boundary layer height from the profiler/RASS measurements, one uses Signal-to-Noise-Ratio (SNR) from the profiler, and the other uses the vertical gradient of virtual potential temperature from RASS. The detected BLH was validated against BLH from rawinsonde measurements. The SNR method gives a better mean BLH in the daytime convective unstable boundary layers while the gradient method shows better correlation with the rawinsonde BLH. The gradient method appears to give better results for the nighttime boundary layers.

The Weather Research and Forecasting (WRF) model simulations were made by the Aerospace Corporation for July, August, and September of 2007 and the output were kindly made available for this thesis study. The model evaluation was made at one point only: the inland location at Miramar (MMR) near San Diego. The model boundary layer height was compared to those from profiler/RASS. Although WRF reasonably predicts the general boundary layer behavior, the WRF forecast thermodynamic field indicates that the boundary layer height in WRF should be lower than the observed BLH by several

hundred meters. However, the BLH output from WRF, diagnosed from the bulk Richardson, is not consistent with the forecast thermodynamic field. Instead of at the forecast inversion base, the diagnosed BLH from WRF is well above the WRF forecast boundary layer. Consequently, although the mean output BLH from WRF only appears to be about 95 to 150 m lower compared to the observed BLH, the actual forecast boundary layer is much lower if the BLH can diagnosed from the model field more accurately.

An alternative BLH detection scheme is proposed and tested for WRF. This is a simple scheme that involves only the potential temperature gradient. This scheme shows significant improvement of the nighttime BLH detection and the scheme improved slightly on the correlation with the BLH detected from the gradient method. The scheme does not give 'better' BLH from WRF in comparison with observation, because it does not change the WRF physical parameterizations for a better forecasted boundary layer, which is not the focus of this study.

B.   RECOMMENDATIONS

An alternative boundary layer height diagnostic scheme should be investigated for both the daytime and nighttime boundary layers since the bulk Richardson number based diagnostic tool does not appear to be effective. More thorough evaluations of the WRF performance in general should be made at different locations within the model domain, such as LAX, MOV, ONT, or SIM (on Figure 24), to give more comparison of the WRF detected BLH at those locations. Along with the data from MMR, all sites combined would give a more thorough investigation into the accuracy of the WRF model derived BLH. Further investigation into the model dynamics and physics should be done in order to improve the forecast of boundary layer thermodynamic properties.

LIST OF REFERENCES

Angevine, W. M., and K. Mitchell, 2001: Evaluation of the NCEP mesoscale eta model convective boundary layer for air quality applications. *Mon. Wea. Rev.,* **129**, 2761-2775.

Bianco, L., J. M. Wilczak, D. Gottas, and A. B. White, 1995: Development of a real-time, automated boundary layer height detection algorithm using radar wind profiler data. CETEMPS-University of L'Aquila; NOAA/Environmental Technology Laboratory, **6.10**, 1-4.

Bianco, L., and J. M. Wilczak, 2002: Convective boundary layer depth: improved measurement by doppler radar wind profiler using fuzzy logic methods. *J. Atmos. Oceanic Technol.,* **19,** 1745-1758.

Cohn, S. A., and W. M. Angevine, 2000: Boundary layer height and entrainment zone thickness measured by lidars and wind-profiling radars. *J Appl. Meteor.,* **39**, 1233-1247.

Coulter, R. L., W. Gao, and B. M. Lesht, 1995: An iterative procedure for estimating areally averaged heat flux using planetary boundary layer mixed layer height and locally measured heat flux. Argonne National Laboratory, Session Papers, 63-65.

Coulter, R. L., and D. J. Holdridge, 1998: A Procedure for the Automatic Estimation of Mixed Layer Height. Argonne National Laboratory, Session Papers, 177-180.

Deardoff, J. W., and E. W. Peterson, 1980: The boundary-layer growth equation with Reynolds averaging. *J. Atmos. Sci.,* **37,** 1405-1409.

Drobinski, P., R. A. Brown, P. H. Flamant, and J. Pelon, 1998: Evidence of organized large eddies by ground-based Doppler lidar, sonic anemometer and sodar. Bound.-Layer Meteor., 88, 343–361.

Eleuterio, D. P., Q. Wang, and K. Rados, 2004: Diagnostic boundary layer height for cloud-topped boundary layers in a mesoscale model, Research Paper, Naval Postgraduate School, Monterey, CA.

Fuzzy Logic Tutorial, 2003/2006: Fuzzy Logic Just For Plain Folks. Thomas Sowell. [Available from http://www.fuzzy-logic.com.] Date last accessed, May/2007.

Grimsdell, A.W., and W. M. Angevine, 1998: Convective boundary layer height measurement with wind profilers and comparison to cloud base. *J. Atmos. Oceanic Technol.,* **15**, 1331-1338.

Helsinki Testbed, 2008: Wind Profiler, Helsinki Testbed. [Available from http://testbed.fmi.fi.] Date last accessed, Feb/2008.

Heo, B; Jacoby-Koaly, S; Kim, K*; Campistron, B; Benech, B; Jung, E, 2003:Use of the Doppler spectral width to improve the estimation of the convective boundary layer height from UHF wind profiler observations, J. Atmos. Ocean. Technol., Vol. 20, no. 3, pp. 408-424.

Hong, S.-Y., and H.-L. Pan, 1996: Nonlocal boundary layer vertical diffusion in a medium-range forecast model. Mon. Wea. Rev., 124, 2322-2339.

Johansson, C. and H. Bergstro, 2005: An auxiliary tool to determine the height of the boundary layer, Bound Layer Meterorol., 115, 423-432.

Johansson, C., Smedman, A., Hőgstrőm, U., Brasseur, J. G., and Khanna, S.: 2001, Critical Test of the Validity of Monin-Obukhov Similarity During Convective Conditions', J. Atmos. Sci., 58, 1549–1566.

Kaimal, J.C., N. L. Abshire, R. B. Chadwick, M.T. Decker, W. H. Hooke, R. A. Kropfli, W. D. Neff, F. Pasqualucci and P.H. Hildebrand, 1982: Estimating the depth of the daytime convective boundary layer. *J. Appl. Meteor.,* **21**, 1123-1129.

L3 Communications Titan Group, 2007: SCIPUFF Dispersion Model. Titan Products and Services. [Available from http://www.titan.com.] Date last accessed, May/2007.

Lee, S. J., H. D. Yoo, and H. Kawai, 2004: Qualitative evaluation of the KMA regional model mixing-depth prediction using wind-profiler signal-to-noise-ratio data. National Weather Prediction Division, Korean Meteorological Administration, **14B.8**, 1-13.

Moore, M. J., 2005: Evolution of boundary layer height in response to surface and mesoscale forcing. M.S. Thesis, Naval Postgraduate School, Monterey, CA, 59 pp.

NCAR, 2006: A description of the advanced research WRF version 2. National Center for Atmospheric Research (NCAR), Mesoscale and Microscale Meteorology Divison, Tech Note TN-468+STR, 88 pp.

Norris, J. R.: 1998, 'Low Cloud Type Over the Ocean from Surface Observations. Part I: Relationship to Surface Meteorology and the Vertical Distribution of Temperature and Moisture', J. Climate 11, 369–382.

OFCM, 2004: Federal Research and Development Needs and Priorities for Atmospheric Transport and Diffusion Modeling. Office of the Federal Coordinator of Meteorological Services and Supporting Research (OFCM), Joint Action Group for ATD Modeling, FCM-R23-2004, 207 pp.

Ottersten, H.: 1969,: Atmospheric Structure and Radar Backscattering in Clear Air, Radio Sci. 4, 1179-1193.

Rao, K. S., 2005: Uncertainty analysis in atmospheric dispersion modeling. *Pure Appl. Geophys.,* **162**, 1894-1917.

Stull, R. B., 1988: An Introduction to Boundary Layer Meteorology. Kluwer Academic, 666 pp.

Therry, G. and P. Lacarrere, 1983: Improving the kinetic energy model for the planetary boundary layer description. *Bound. Layer. Moteorl.*, **25**, 63-88.

University of Wisconsin, 1996: Radiosondes. Edward J. Hopkins. [Available from http://www.aos.wisc.edu/.] Date last accessed, Feb/2008.

Vogelezang, D. H. P., and A. A. M. Holtslag, 1996: Evaluation and model impacts of alternative boundary-layer height formulations. Bound.-Layer Meteor., 81, 245–269.

White, A.B., Fairall, C.W., and Thompson, D.W.: 1991a, 'Radar Observations of Humidity Variability In and Above the Marine Atmospheric Boundary Layer', J. Atrnos. Ocean. Technol. 8, 639-558.

White, A. B., Fairall, C.W., and Wolfe, D.E.: 1991b, 'Use of 915 MHz Wind Profiler Data to Describe the Diurnal Variability of the Mixed Layer', in Preprints, 7th Joint Conference on Applications of Air Pollution Meteorology with AWMA, New Orleans, Jan. 14-18, 1991, Amer. MeteoroI. Soc., pp. J161-J166.

White, A. B. : 1993, 'Mixing Depth Detection Using 915-MHz Radar Reflectivity Data', in Preprints, 8th Symposium on Meteorological Observations and Instrumentation, Anaheim, California, Jan. 17-22, 1993, Amer. Meteorol. Soc., 248-250.

Yi, C., K. J. Davis, B. W. Berger, and P. S. Bakwin, 2001: Long-term observations of the dynamics of the continental planetary boundary layer. *J. Atmos. Sci.,* **58**, 1288-1299.

Zeng, X; Brunke, MA; Zhou, M; Fairall, C; Bond, NA; Lenschow, DH, 2004: Marine Atmospheric Boundary Layer Height over the Eastern Pacific: Data Analysis and Model Evaluation, Journal of Climate [J. Clim.]. Vol. 17, no. 21, 4159-4170. Nov 2004.

THIS PAGE INTENTIONALLY LEFT BLANK

INITIAL DISTRIBUTION LIST

1.   Defense Technical Information Center
        Ft. Belvoir, Virginia

2.   Dudley Knox Library
        Naval Postgraduate School
        Monterey, California

3.   Air Force Technical Applications Center
        TMAR
        Patrick AFB, Florida

4.   The Aerospace Corporation
        Leslie Belsma
        El Segundo, California

5.   Air Force Weather Agency
        Maj Timothy Nobis
        Offutt AFB, Nebraska

6.   Army Research Lab
        Walter Bach
        Adelphia, Maryland